REPORT DOCUMENTATION PAGE

Form Approved
OMB NO. 0704-0188

1. AGENCY USE ONLY (Leave Blank)	2. REPORT DATE	3. REPORT TYPE AND DATES COVERED
	April 30, 2004	Final Report (8/1/00--1/31/04)

4. TITLE AND SUBTITLE
Analysis and Control of High-Speed Wheeled Mobile Robots

5. FUNDING NUMBERS
DAAD19-00-1-0473

6. AUTHOR(S)
Prof. Panagiotis Tsiotras

7. PERFORMING ORGANIZATION NAME(S) AND ADDRESS(ES)
Georgia Institute of Technology, Atlanta, GA 30332-0150

8. PERFORMING ORGANIZATION REPORT NUMBER

9. SPONSORING / MONITORING AGENCY NAME(S) AND ADDRESS(ES)
U. S. Army Research Office
P.O. Box 12211
Research Triangle Park, NC 27709-2211

10. SPONSORING / MONITORING AGENCY REPORT NUMBER
40298.1-C1

11. SUPPLEMENTARY NOTES
The views, opinions and/or findings contained in this report are those of the author(s) and should not be construed as an official Department of the Army position, policy or decision, unless so designated by other documentation.

12 a. DISTRIBUTION / AVAILABILITY STATEMENT
Approved for public release; distribution unlimited.

12 b. DISTRIBUTION CODE

13. ABSTRACT (Maximum 200 words)

The overall objective of this research was to contribute to the development of control algorithms for autonomous high-speed vehicles moving in uncertain and/or off-road environments. The motivation behind this research objective was the need of ``intelligent" drivers that can be used to navigate and guide an autonomous vehicle in a high-threat environment, perform its assigned task, while at the same time minimizing exposure to potential threats and hazards. Given the previous overall objective, this research has focused on two areas: First, on the development of simple, albeit accurate, mathematical models for the complex behavior arising between the wheel tires and the ground. The study of tire friction dynamics is brought about by the need of high-speed operation of the vehicle. Our developed tire friction models are solidly based on first physical principles; they also capture transient dynamics which are important during high-speed and/or continuously changing driving conditions. Second, on the development of optimal, maximum-velocity and minimum-time driving maneuvers (``optimal driving primitives") under friction constraints. These results are also novel in the sense that the tire/ground nonlinearities (i.e., saturating friction) are explicitly accounted for. The numerical simulations show very realistic behavior of the vehicle trajectory, in the sense that sliding and skidding is often induced by the optimizer in order to achieve the control objective. This is not unlike the action of an expert human race driver who typically induces skidding and/or sliding to minimize time or maximize exit velocity from a corner.

14. SUBJECT TERMS	15. NUMBER OF PAGES
Mobile Robots, Unmanned Vehicles, Navigation, Tire Friction, Optimization	35
	16. PRICE CODE

17. SECURITY CLASSIFICATION OR REPORT	18. SECURITY CLASSIFICATION ON THIS PAGE	19. SECURITY CLASSIFICATION OF ABSTRACT	20. LIMITATION OF ABSTRACT
UNCLASSIFIED	UNCLASSIFIED	UNCLASSIFIED	UL

NSN 7540-01-280-5500

Standard Form 298 (Rev.2-89)
Prescribed by ANSI Std. 239-18
298-102

Enclosure 1

Analysis and Control of High-Speed Wheeled Mobile Robots

Final Report

ARO Grant Number DAAD19-00-1-0473

by

Panagiotis Tsiotras
Principal Investigator
School of Aerospace Engineering
Georgia Institute of Technology
Atlanta, GA 30332-0150

for

U.S. Army Research Office
Systems and Control
Computing and Information Science Division
P.O. Box 12211
4300 South Miami Blvd.
Research Triangle Park, NC 27709-2211

Attention

Dr. Randy Zachery
Tel: (919) 549-4368
E-mail: randy.zachery@us.army.mil

April 2004

School of Aerospace Engineering
Atlanta, Georgia 30332-0150 U.S.A.
PHONE 404-894-9526
FAX 404-894-2760

ANALYSIS AND CONTROL OF HIGH-SPEED WHEELED MOBILE ROBOTS

Final Report

ARO Grant Number DAAD19-00-1-0473

Panagiotis Tsiotras
Principal Investigator
School of Aerospace Engineering
Georgia Institute of Technology
Atlanta, GA 30332-0150

Executive Summary

Therein we summarize the research results developed under ARO Grant number DAAD19-00-1-0473. The period of performance for this research award was from August 2000 to January 2004.

The overall objective of this research was to contribute to the development of control algorithms for autonomous high-speed vehicles moving in uncertain and/or off-road environments. The motivation behind this research objective was the need of "intelligent" drivers that can be used to navigate and guide an autonomous vehicle in a high-threat environment, perform its assigned task (e.g., drop a munition or shoot a projectile), while at the same time minimizing exposure to potential threats and hazards.

Given the previous overall objective, this research has focused on two areas: First, on the development of simple, albeit accurate, mathematical models for the complex behavior arising between the wheel tires and the ground. The study of tire friction dynamics is brought about by the need of high-speed operation of the vehicle. These friction dynamics determine the forces acted upon the vehicle. In contrast to all other empirical results in the literature (most of which are valid only at steady-state), our developed tire friction models are solidly based on first physical principles; they also capture transient dynamics which are important during high-speed and/or continuously changing driving conditions. Second, on the development of optimal, maximum-velocity and minimum-time driving maneuvers ("optimal driving primitives") under friction constraints. These results are also novel in the sense that the tire/ground nonlinearities (i.e., saturating friction) are explicitly accounted for. The numerical simulations show very realistic behavior of the vehicle trajectory, in the sense that sliding and skidding is often induced by the optimizer in order to achieve the control objective. This is not unlike the action of an expert human race driver who typically induces skidding and/or sliding to minimize time or maximize exit velocity from a corner.

As a result of the support received from this award, two students received their M.S. degrees and one student will soon receive his Ph.D. Two book chapters, four archival journal publications and eight conference papers document the results of this work.

Contents

List of Figures

List of Tables

1 Introduction

1.1 Motivation and Problem Statement

The need for reducing the risk for human lives in operating machines in hazardous or hostile environments has lead to the development of unmanned and often autonomous vehicles for both commercial and military applications. The demand for completely autonomous machines and vehicles rises from the need for maximum performance and minimum error during operation which requires the elimination of the 'human factor' in the control loop.

A class of vehicles that we envision to be completely automated in the future are ground wheeled vehicles (Fig. 1) that operate in hostile off-road environments (e.g., battlefields). A typical mission would be to drive the vehicle from point A to point B, avoiding any obstacles and minimizing the exposure to danger (Fig. 1). In general, minimization of the exposure to danger involves driving through the trajectory in minimum time or maximum average velocity.

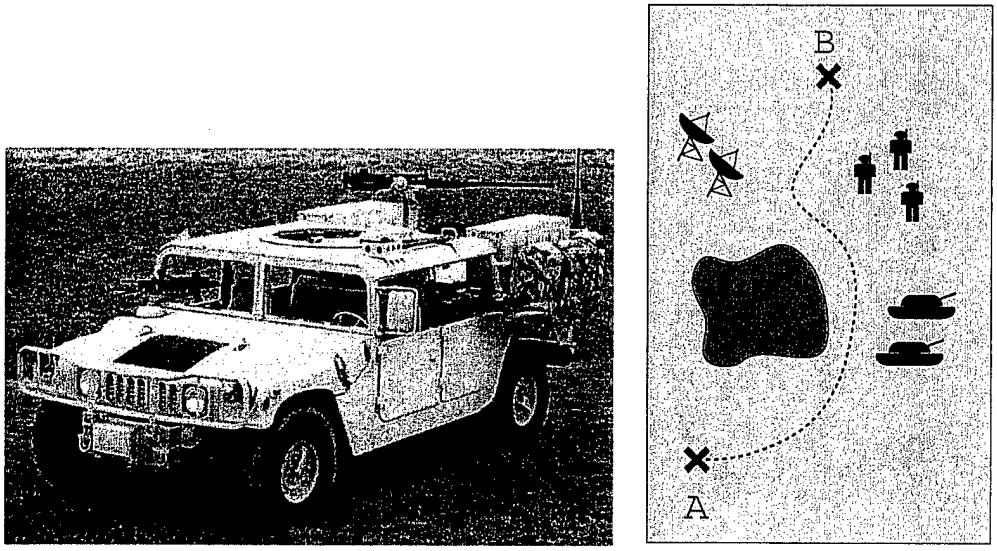

Figure 1: Military Off-Road Vehicle and Mission Map.

The fastest off-road vehicles can be found in rally-cross races. Racing such a vehicle requires a great deal of practice and skill. In this research our plan is to develop controllers that operate as "intelligent rally/race-drivers" and imitate the driving techniques of race drivers that differ substantially from the techniques used by everyday drivers. It is evident, even to inexperienced drivers, that race driving involves operating the vehicle at the limits of its handling capacity. For example, race drivers intentionally use skidding through corners to optimize their trajectory as far as travel time and velocity, and minimize reaction time of the vehicle for the next maneuver (Fig. 2). Such regions of operation are avoided by everyday drivers because of safety. Maneuvers in these regions require a great deal of skill to be performed in a controlled manner. Actually, the automotive industry's research focuses in developing control systems to prevent commercial vehicles from reaching such limits of operation. The situation is redically different for autonomous/unmanned military vehicles, where the primary objective is success of the mission.

Before delving into the problem of designing "expert driving software agents" it is imperative to

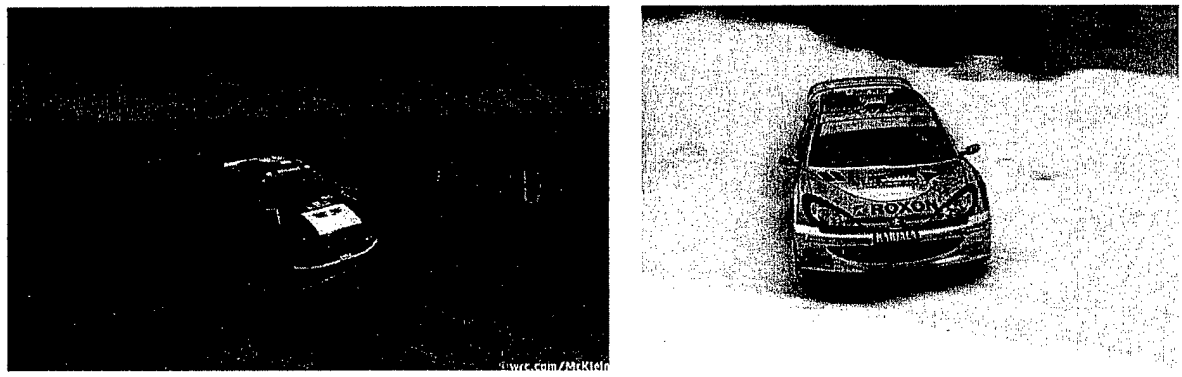

Figure 2: Rally-Race driving involves driving the race car to its handling limits. Race drivers intentionally invoke skidding in corners to optimize the trajectory and minimize reaction time for the maneuver to come.

have a very good characterization of the forces developed between the vehicle wheels and the ground, as these forces are the main mechanism for controlling the vehicle. Previous results in the area of mobile robots have used several simplifying assumptions. A typical scenario involves a commanded (off-line) trajectory, communicated to the robot, and an on-board tracking control law to follow this trajectory in real-time. In essence, the trajectory generation and trajectory tracking problems are treated independently, based on the assertion that the vehicle will be successful in following the commanded path with arbitrary accuracy. Unfortunately, reality is not that accommodating. Neglected tire/ground dynamics may have a profound effect in the performance of the overall system. Therefore, in the past, control development for autonomous wheeled vehicles has been performed under the ideal assumption of no-slipping/no-sliding conditions. This no-slip/no-sliding assumption cannot be guaranteed *a priori* and, as a result, kinematic models developed under this ideal assumption are not accurate. In fact, no-slippage/no-skidding is never satisfied in practice as slippage is what actually generates friction [8]. In the extreme cases of interest to this research (i.e., high-speed driving, cornering with braking, etc) these simplistic models are inadequate to describe, even qualitatively, the ensuing motion; see for example Fig. 2.

Driving under extreme (high-speed, high-load) conditions is a challenging problem. In particular, kinematic models of the vehicle (i.e., models where the wheel velocity is the control input) are inadequate. Dynamic models (i.e., where the control input is the torque delivered to the wheels) are needed instead. These models must be accompanied by reasonably accurate tire models to correctly predict the forces generated by the tires. Very accurate tire models have been developed for this purpose and used for vehicle simulation studies by car and tire manufacturers. However, these tire models are much too complex to be used for control purposes.

Our research has focused on two areas: First, the understanding of the complex friction characteristics arising between the wheel tires and the ground. Departing from all prior major results in the literature we have proposed *dynamic* tire friction models that: (i) are solidly based on first physical principles; (ii) capture transient dynamics which are important during high-speed and/or continuously changing driving conditions; and (iii) are simple enough to be used for control and friction estimation purposes. Second, the development of optimal maximum-velocity and minimum-time driving maneuvers ("optimal driving primitives") under friction constraints. These results are also novel in the sense that the tire/ground nonlinearities (i.e., saturating friction) are explicitly accounted for. The numerical simulations show very realistic behavior of the vehicle trajectory, in

the sense that sliding and skidding is often induced by the optimizer in order to achieve the control objective. This is not unlike the action of an expert human race driver who typically induces skidding and/or sliding to minimize time or maximize exit velocity from a corner; see Fig. 2.

1.2 Goals of this Report

The main goal of this report is to summarize the results obtained under this research program. Since most of the technical results have appeared or will soon appear in over 15 archival journal and conference publications, below we only summarize these results and remark on their significance and their interrelationship.

2 Summary of Work Accomplished

The following research accomplishments were achieved over the duration of this project (August 2000–January 2004).

2.1 Theoretical Development and Experimental Validation of Mobile Robot Control Laws

The assumption of no-slipping/no-slidding induces nonholonomic constraints in the motion of the vehicle. Even for this simplified case, the available control laws have not been compared in the past. In this work we performed a comprehensive investigation of several controllers developed in the literature for the special case of unicycle-type, nonholonomic wheeled mobile vehicles. In particular, we compared controllers from the two major classes of stabilizing controllers for these vehicles. Namely, time-varying controllers [9, 10, 11, 12, 13] and time-invariant, discontinuous controllers [14, 15, 16, 17, 18, 19, 20].

A comparative study of controllers for nonholonomic systems and, in particular, between time-varying and time-invariant controllers, had not been done in the literature prior to [1]. Moreover, the robustness properties of these controllers is still a topic under investigation. Our work provided a step towards this goal by comparing the stabilization and robustness properties of several time-varying and time-invariant controllers for a wheeled robot.

Six controllers were tested. Two of them were time-invariant [16, 17] and the rest were time-varying (periodic) [12, 13, 9, 21]. Table 1 summarizes the controllers tested. All these controllers were implemented on a unicycle-type robot called Khepera, shown in Fig. 3(b).

The Khepera robot is a product of the K-Team (`http://www.k-team.com`). It is a mobile robot with two DC motor-driven wheels. The DC motors are connected to the wheels through a 25:1 reduction gear box. Two incremental encoders are placed on the motor axes. The resolution of each encoder is 24 pulses per revolution of the motor axis. This corresponds to $24 \times 25 = 600$ pulses per revolution of the wheels or 12 pulses per millimeter of wheel displacement. The algorithm for estimating the velocity from the encoder outputs is implemented on the robot. For DC motor speed control, a native PID controller is implemented on the Khepera robot. All one then needs to do in order to control Khepera, is to read position signals and issue velocity commands via the RS-232 serial port. The maximum sampling rate can be upto 100Hz owing to the limitation of the RS-232 serial communication (maximum is 4.8kbytes/s for the Khepera robot). For all experiments a 50Hz sampling was used.

Table 1: Controllers Tested

Controller	Ref.	Comments
1	[22, 20]	Discontinuous, Exponential Convergence
2	[18, 20]	Discontinuous, Bounded, Exponential Convergence
3	[16]	Two-stage switching, Time-Invariant controller
4	[17]	Time-Invariant, Polar Coordinates
5	[12]	Time-Varying
6	[13]	Time-Varying
7	[9]	Time-Varying
8	[21]	Time-Varying, Exponential Convergence

The Khepara robot introduces many realistic difficulties, such as different motor dynamics for the two wheels, time delay, quantization, sensor noise and saturation. The performance of each controller was tested with respect to convergence characteristics, speed of response, steady-state error, robustness to sensor noise, etc. Suggestions on how to improve each controller's performance were also presented.

In addition to the six controllers of Table 1, two new controller for unicycle-type vehicles was proposed. The first controller is given by

$$u_1 = -kx_1 + \mu \frac{s(x)}{x_1^2 + x_2^2} x_2, \quad u_2 = -kx_2 - \mu \frac{s(x)}{x_1^2 + x_2^2} x_1 \tag{1}$$

where s is given by $s(x) := x_3 - (1/2)x_1x_2$. The derivative of s is readily calculated as

$$2\dot{s} = x_1u_2 - u_1x_2 \tag{2}$$

Here x_1, x_2 and x_3 are given by (see also Fig. 3(b))

$$\begin{aligned} x_1 = x\cos\gamma + y\sin\gamma, \quad x_2 = \gamma, \\ x_3 = x\sin\gamma - y\cos\gamma \end{aligned} \tag{3}$$

A modification of the control law (1) in a neighborhood of the x_3-axis is necessary, since this control law is not defined when $x_1 = x_2 = 0$. The modification used here is similar to the one presented in [15]. The idea is to create a region around the x_3-axis where the control law (1) is not used. To this end, let the region $\mathcal{D}_{\bar{\eta}}^b = \{(x_1, x_2, x_3) : |\eta| \geq \bar{\eta}\}$ where

$$\eta := \frac{s}{\sqrt{x_1^2 + x_2^2}} = \frac{s}{\nu} \tag{4}$$

With a slight abuse of notation, we let $\mathcal{D}_{\infty}^b$ denote the set $\mathcal{D}_{\infty}^b = \{(x_1, x_2, x_3) : \nu = 0,\ s \neq 0\} = \{(x_1, x_2, x_3) : x_1 = x_2 = 0,\ x_3 \neq 0\}$. In the set $\mathcal{D}_{\bar{\eta}}^b$, where $|\eta|$ is "large" we can apply, for instance, the control law, $u_1 = k_s\text{sgn}(s)$ and $u_2 = 0$ where k_s is some constant chosen by the user. A simple

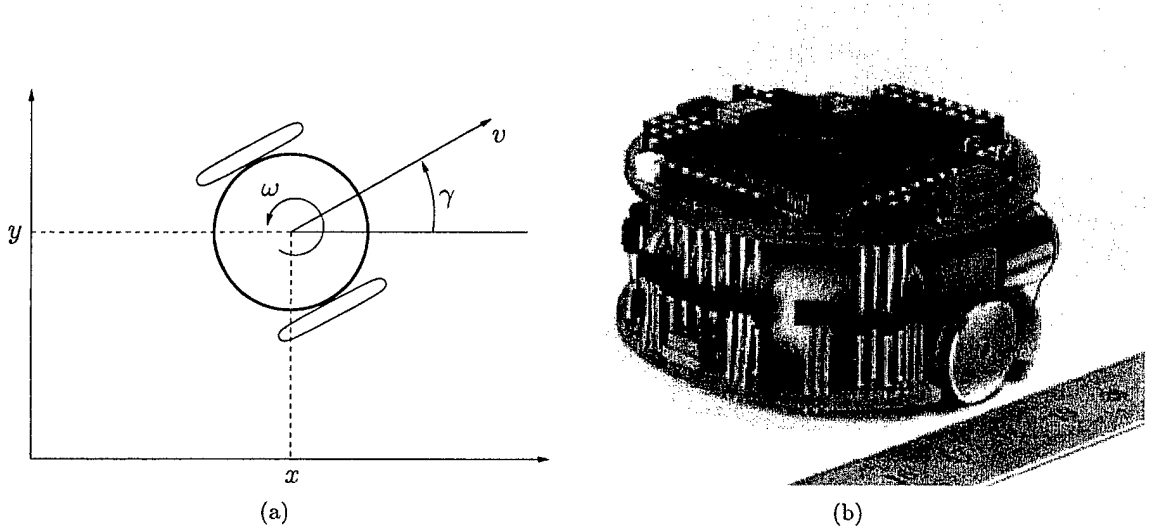

(a) (b)

Figure 3: (a) Definition of configuration variables, (b) The Khepera robot.

calculation shows that with this control law the system will leave $\mathcal{D}_{\bar{\eta}}^b$ in finite time. Moreover, it can be easily shown that the region $\mathcal{D}_{\bar{\eta}}^g := \Re^3 \backslash \mathcal{D}_{\bar{\eta}}^b$ is invariant. Thus, once the system enters $\mathcal{D}_{\bar{\eta}}^g$ stays there for all future times. Once in $\mathcal{D}_{\bar{\eta}}^g$, the control law (1) can be used.

The second controller is given by

$$u_1 = -k\frac{x_1}{\sqrt{\nu^2+1}} + \mu\,\mathrm{sat}_2(s,\nu), \quad u_2 = -k\frac{x_2}{\sqrt{\nu^2+1}} - \mu\,\mathrm{sat}_1(s,\nu) \tag{5}$$

where $\nu = \sqrt{x_1^2 + x_2^2}$ and k and μ are constants satisfying

$$\mu > 2k > 0, \quad \text{if } |\eta| < 1 \tag{6a}$$

$$\mu > -2k > 0, \quad \text{if } |\eta| \geq 1 \tag{6b}$$

The saturation functions sat_i $(i = 1, 2)$ are defined as

$$\mathrm{sat}_i(s,\nu) = \begin{cases} \mathrm{sat}\left(\frac{s}{\nu}\right)\frac{x_i}{\nu} & \text{if} \quad \nu \neq 0 \\ \mathrm{sgn}(s) & \text{if} \quad \nu = 0 \end{cases} \tag{7}$$

where $\mathrm{sat}(x) := \min\{1, |x|\}\mathrm{sgn}(x)$.

Figures 4 and 5 show selected trajectories with the control laws (1) and (5). Table 2 summarizes the experimental results of all controllers tested. In Table 2 the letters 'E', 'N', 'S' and 'L' stand for Easy, Normal, Singular and Long-distance missions respectively. 'E' stands for 'Excellent' which means good speed of response, no oscillations either in x, y or γ, reasonable control inputs and "natural" trajectories. 'G' stands for 'Good', which means that the convergence is acceptable, i.e., within 10 seconds. "S' stands for 'Slow', which means that it took the robot more than 20 seconds to converge. 'C' stands for 'Chattering', which means that trajectories converged, but there was too much chattering in the velocity commands. 'O' stands for 'Oscillatory', which means that the trajectory oscillated around the origin. 'U' stands for unstable/unsatisfactory response.

As indicated by the table, Controller 2 gave the most satisfactory performance for all missions. Its speed of response and the velocity commands were always within acceptable limits. The implementation complexity of all controllers was comparable, with the discontinuous Controller 1 and 3

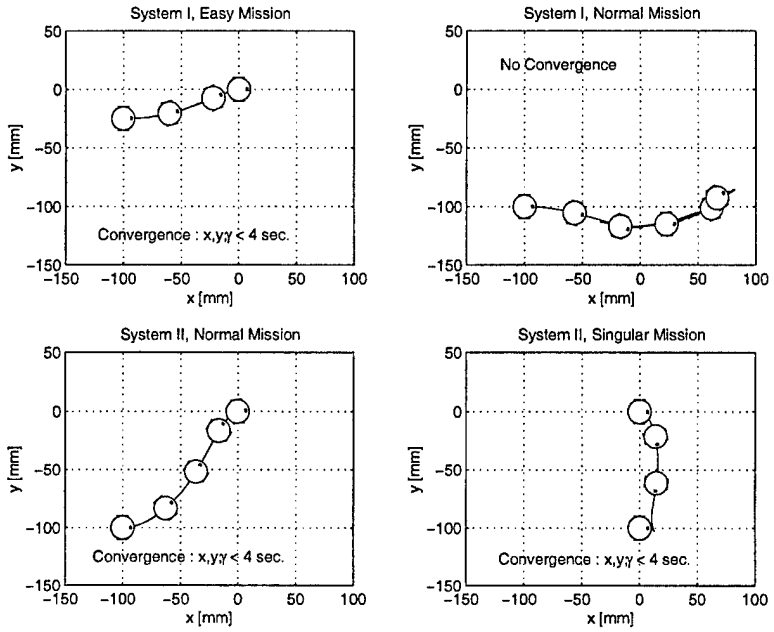

Figure 4: Selected trajectories for Controller 1; from [1].

requiring the most care to avoid singularities. Controller 2 has a built-in mechanism that avoids singular regions. Controllers 2 and 4 generated natural trajectories, i.e., similar to what a human operator would attempt. However, Controller 4 was sensitive to sensor noise resulting in relatively large limit cycles of the heading angle around the origin. Time-varying controllers generated oscillatory paths and all of them showed slow convergence, especially close to the origin. Among the time-varying controllers, Controller 8 exhibited the best performance and speed of response. The implementation of this controller presented the most difficulties, however, because of the requirement to update the parameter λ of the dilation operator (see [21]) using a Newton method at each time step.

The results of this work have been documented in [1, 23, 24].

2.2 Development of Dynamic Friction Models for Longitudinal Motion

The problem of predicting the friction force between the tire and the ground for wheeled vehicles is of enormous importance to automotive industry. Since friction is the major mechanism for generating forces on the vehicle, it is extremely important to have an accurate characterization of the magnitude (and direction) of the friction force generated at the ground/tire interface. However, accurate tire/ground friction models are difficult to obtain analytically. Subsequently, in the past several years, the problem of modeling and predicting tire friction has become an area of intense research in the automotive community. In particular, ABS and traction control systems, that enhanced the safety of modern passenger vehicles, rely on knowledge of the friction characteristics. Traction control systems reduce or eliminate excessive slipping or sliding during vehicle acceleration and thus enhance the controllability and maneuverability of the vehicle. Traction control aims to achieve maximum torque transfer from the wheel axle to forward acceleration. Similarly, anti-lock braking systems (ABS) prohibit wheel lock and skidding during braking by regulating the pressure

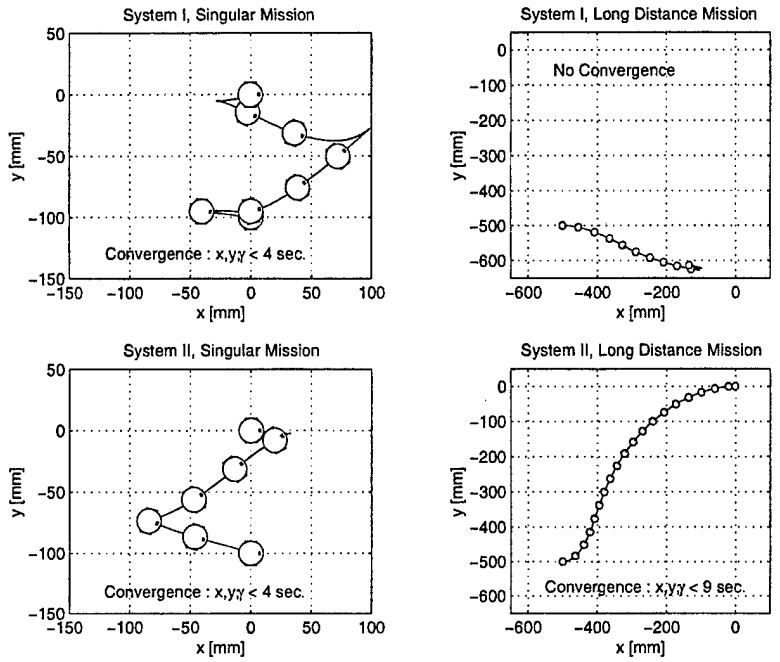

Figure 5: Selected trajectories for Controller 2; from [1].

applied on the brakes, thus increasing lateral stability and steerability, especially during wet and icy road conditions. As with the case of traction control, the main difficulty in designing ABS systems is the nonlinearity and uncertainty of the tire/road models. In either case, the friction force at the tire/road interface is the main mechanism for converting wheel angular acceleration or deceleration (due to the motor torque or braking) to forward acceleration of deceleration (longitudinal force).

A common assumption in most tire friction models is that the normalized tire friction μ

$$\mu = \frac{F}{F_n} = \frac{\text{Friction force}}{\text{Normal force}}$$

is a nonlinear function of the normalized relative velocity between the road and the tire (slip coefficient s) with a distinct maximum; see Fig. 6. In addition, it is understood that μ also depends on the velocity of the vehicle and road surface conditions, among other factors (see [25] and [2]). The curves shown in Fig. 6 illustrate how these factors influence the shape of μ.

The curves shown in Fig. 6 are derived empirically, based solely on steady-state (i.e., constant linear and angular velocity) experimental data [2, 26] in a highly controlled laboratory environment or using specially designed test vehicles. Under such steady-state conditions, experimental data seem to support the force vs. slip curves of Fig. 6. In reality, the linear and angular velocities can never be controlled independently and hence, such idealized steady-state conditions are not reached except during the rather uninteresting case of cruising with constant speed. The development of the friction force at the tire/road interface is very much a dynamic phenomenon. In other words, the friction force does not reach its steady-state value shown in Fig. 6 instantaneously, but rather exhibits transient behavior which may differ significantly from its steady-state value. Experiments performed in commercial vehicles, have shown that the tire/road forces do not necessarily vary along the curves shown Fig. 6, but rather "jump" from one value to another when these forces are displayed in the $\mu - s$ plane [27]. In addition, in realistic situations, these variations are most likely

Table 2: Summary of Experimental Results.

Ctr.	Sys.	E	N	S	L	Note
1	I	E	O	O	O	Oscillatory
	II	E	E	E	E	Good/Fast
2	I	E	O	O	O	Oscillatory
	II	E	E	E	E	Good/Fast/Bounded
3	I	C	C	C	O	Chattering
	II	C	C	C	C	
4	Polar	E in x, y, O in γ				Good/Fast/Noise
5	I/II	G	S	S	O	Very Slow
6	I	U	U	U	U	Diverged
	II	S	S	S	S	Very Slow
7	I/II	S	S	S	O	Very Slow
8	I/II	G	G	G	G	Good/Slow

to exhibit hysteresis loops, clearly indicating the dynamic nature of friction.

In this work, we studied in detail the existing tire friction models in the literature and we developed a new, velocity-dependent, dynamic friction model that can be used to describe the tire/road interaction for the longitudinal motion of a vehicle. The proposed model has the advantage that is developed starting from first principles based on a simple, point-contact dynamic friction model [28]. The parameters entering the model have a physical significance allowing the designer to tune the model parameters using experimental data. The proposed friction model is also velocity-dependent, a property that agrees with experimental observations. A simple parameter in the model can also be used to capture the road surface characteristics. Finally, in contrast to many other static models, our model is shown to be well-defined everywhere (even at zero rotational or linear vehicle velocities) and hence, is appropriate for any vehicle motion situations as well as for control law design. This is especially important during transient phases of the vehicle operation, such as during braking or acceleration.

The proposed tire friction model starts from the generalization of the following point contact friction model as proposed in [29]

$$\dot{z} = v_r - \frac{\sigma_0 |v_r|}{g(v_r)} z \tag{8}$$

$$F = (\sigma_0 z + \sigma_1 \dot{z} + \sigma_2 v_r) F_n \tag{9}$$

with

$$g(v_r) = \mu_c + (\mu_s - \mu_c) e^{-|v_r/v_s|^\alpha} \tag{10}$$

where σ_0 is the rubber longitudinal lumped stiffness, σ_1 the rubber longitudinal lumped damping, σ_2 the viscous relative damping, μ_c the normalized Coulomb friction, μ_s the normalized static friction, $(\mu_c \leq \mu_s)$, v_s the Stribeck relative velocity, F_n the normal force, $v_r = r\omega - v$ the relative velocity, and z the internal friction state. The constant parameter α is used to capture the steady-steady friction/slip characteristic[1].

[1]The model in (9) differs from the point-contact LuGre model in [28] in the way that the function $g(v)$ is defined. Here we propose to use $\alpha = 1/2$ instead of $\alpha = 2$ as in the LuGre point-contact model in order to better match the pseudo-stationary characteristic of this model (map $s \mapsto F(s)$) with the shape of the Pacejka's model.

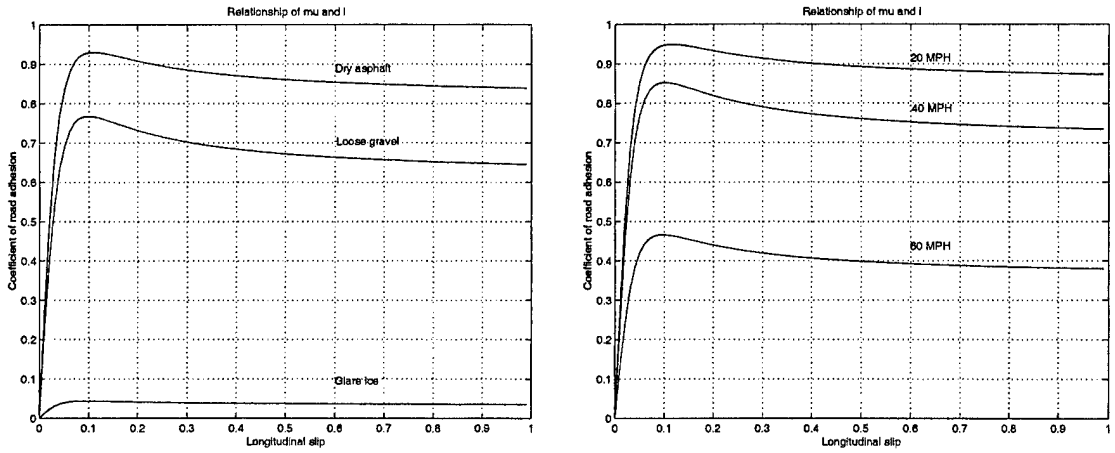

(a) (b)

Figure 6: Typical variations of the tire/road friction profiles for different road surface conditions (a), and different vehicle velocities (b). Curves given by Harned et al. [2].

We have extended the point friction model (8)-(9) to a distributed friction model along the patch by letting $z(\zeta,t)$ denote the friction state (deflection) of the bristle/patch element located at the point ζ along the patch at a certain time t. At every time instant $z(\zeta,t)$ provides the deflection distribution along the contact patch. The model (8)-(9) can now be written as

$$\frac{\mathrm{d}\,z}{\mathrm{d}t}(\zeta,t) = v_r - \frac{\sigma_0|v_r|}{g(v_r)}\,z \tag{11}$$

$$F = \int_0^L dF(\zeta,t)\,, \tag{12}$$

with $g(v_r)$ defined as in (10) and where

$$\mathrm{d}F(\zeta,t) = \left(\sigma_0\,z(\zeta,t) + \sigma_1\,\frac{\partial z}{\partial t}(\zeta,t) + \sigma_2 v_r\right)\mathrm{d}F_n(\zeta,t)\,,$$

where $\mathrm{d}F(\zeta,t)$ is the differential friction force developed in the element $\mathrm{d}\zeta$ and $\mathrm{d}F_n(\zeta,t)$ is the differential normal force applied in the element $\mathrm{d}\zeta$ at time t. This model assumes that the contact velocity of each differential state element is equal to v_r.

Assuming a steady-state normal force distribution $\mathrm{d}F_n(\zeta,t) = \mathrm{d}F_n(\zeta)$ and introducing a normal force density function $f_n(\zeta)$ (force per unit length) along the patch, i.e.,

$$\mathrm{d}F_n(\zeta) = f_n(\zeta)\mathrm{d}\zeta$$

one obtains the total friction force as

$$F(t) = \int_0^L (\sigma_0 z(\zeta,t) + \sigma_1\frac{\partial z}{\partial t}(\zeta,t) + \sigma_2 v_r) f_n(\zeta)\mathrm{d}\zeta \tag{13}$$

Noting that[2] $\dot{\zeta} = |r\omega|$, and that

$$\frac{\mathrm{d}\,z}{\mathrm{d}t}(\zeta,t) = \frac{\partial z}{\partial \zeta}\frac{\partial \zeta}{\partial t} + \frac{\partial z}{\partial t},$$

[2]It is assumed here that the origin of the ζ-frame changes location when the wheel velocity reverses direction, such that $\dot{\zeta} = r\omega$, for $\omega > 0$, and $\dot{\zeta} = -r\omega$, for $\omega < 0$.

we have that equation (11) describes a partial differential equation, i.e.

$$\frac{\partial z}{\partial \zeta}(\zeta,t)\,|r\omega| + \frac{\partial z}{\partial t}(\zeta,t) = v_r - \frac{\sigma_0|v_r|}{g(v_r)}\,z(\zeta,t) \tag{14}$$

that should be solved in both in time and space.

The time steady-state characteristics of the model (11)-(12) are obtained by setting $\frac{\partial z}{\partial \zeta}(\zeta,t) \equiv 0$ and by imposing that the velocities v and ω are constant. A simple calculation shows that

$$z_{ss}(\zeta) \;=\; \mathrm{sgn}(v_r)\frac{g(v_r)}{\sigma_0}\left(1 - e^{-\frac{\sigma_0}{g(v_r)}\left|\frac{v_r}{\omega r}\right|\zeta}\right) = c_2(1 - e^{c_1\zeta}) \tag{15}$$

where

$$c_1 = -\frac{\sigma_0}{g(v_r)}\left|\frac{v_r}{\omega r}\right|, \qquad c_2 = \mathrm{sgn}(v_r)\frac{g(v_r)}{\sigma_0} \tag{16}$$

Notice that when $\omega = 0$ (locked wheel case) the distributed model, and hence the steady-state expression (15) collapses into the one predicted by the standard point-contact LuGre model. This agrees with the expectation that for a locked wheel the friction force is only due to pure sliding.

The steady-state value of the total friction force is calculated from (13)

$$F_{ss} = \int_0^L (\sigma_0 z_{ss}(\zeta) + \sigma_2 v_r) f_n(\zeta)\, d\zeta \tag{17}$$

and it depends on the normal force distribution. For example, for the constant distribution case, we have that $F_{ss}(s)$, can be computed as:

- *Driving case.* In this case $v < r\omega$, and the force at steady-state is given by

$$F_d(s) = \mathrm{sgn}(v_r)F_n g(s)\left(1 + \frac{g(s)}{\sigma_0 L|s|}(e^{-\frac{\sigma_0 L|s|}{g(s)}} - 1)\right) + F_n\sigma_2 r\omega s \tag{18}$$

  with $g(s) = \mu_c + (\mu_s - \mu_c)\,e^{-|r\omega s/v_s|^\alpha}$, for some constant ω, and $s = 1 - \frac{v}{r\omega}$.

- *Braking case.* Noticing that the following relations hold between the braking s_b and the driving s_d slip definitions,

$$r\omega s_d = v s_b, \qquad s_d = \frac{s_b}{s_b + 1}$$

  the steady-state friction force for the braking case can be written as

$$F_b(s) = \mathrm{sgn}(v_r)F_n g(s)\left(1 + \frac{g(s)|1+s|}{\sigma_0 L|s|}(e^{-\frac{\sigma_0 L|s|}{g(s)|1+s|}} - 1)\right) + F_n\sigma_2 v s \tag{19}$$

  where $g(s) = \mu_c + (\mu_s - \mu_c)\,e^{-|vs/v_s|^\alpha}$, for constant v, and $s = \frac{r\omega}{v} - 1$.

Note that the above expressions depend not only on the slip s, but also on either the vehicle velocity v or the wheel velocity ω, depending on the case considered (driving or braking). Therefore static plots of F vs. s can only be obtained for a specified (constant) velocity. This dependence of the steady-state force/slip curves on vehicle velocity is evident in experimental data found in the literature. Nonetheless, it should be stressed here that it is impossible to reproduce such a curves

form experimental data obtained from standard vehicles during normal driving conditions, since v and ω cannot be independently controlled. For that, specially design equipment is needed. Figure 7(a) shows the steady-state dependence on the vehicle velocity for the braking case, using the data given in Table 3.

Figure 7(a) shows the steady-state dependence on the vehicle velocity for the braking case, using the data given in Table 3.

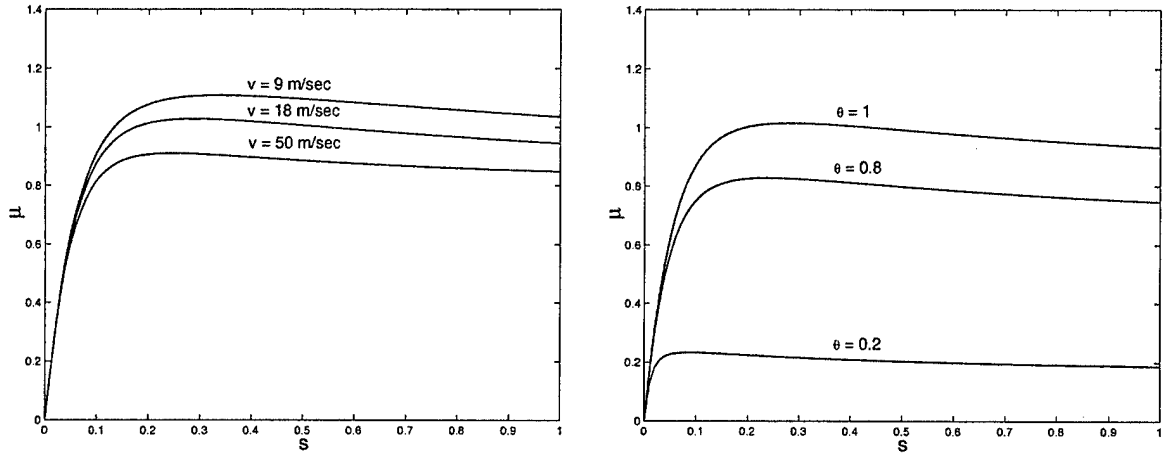

(a) (b)

Figure 7: Static view of the distributed LuGre model with uniform force distribution (braking case) under: (a) different values for v, (b) different values for θ with $v = 20\,\mathrm{m/s} = 72\,\mathrm{Km/h}$. These curves show the normalized friction $\mu = F(s)/F_n$, as a function of the slip velocity s.

Table 3: Data used for the plots in Fig. 7

Parameter	Value	Units
σ_0	181.54	[1/m]
σ_2	0.0018	[s/m]
μ_c	0.8	[-]
μ_s	1.55	[-]
v_s	6.57	[m/s]
L	0.2	[m]

It is clear that the distributed model captures reality better than the lumped, point contact model. It is also clear that in order to use the distributed model for control purposes it is necessary to choose a discrete number of states to describe the dynamics for each tire. This has the disadvantage that a possibly large number of states is required to describe the friction generated at each tire. Alternatively, one could define a *mean friction state* $\bar{z}$ for each tire and then derive an *ordinary differential equation* for $\bar{z}$. This will simplify the analysis and can also lead to much simpler control design synthesis procedures for tire friction problems.

To this end, let us define

$$\bar{z}(t) \equiv \frac{1}{F_n}\int_0^L z(\zeta,t)f_n(\zeta)d\zeta \tag{20}$$

where F_n is the total normal force, given by

$$F_n = \int_0^L f_n(\zeta)\, d\zeta$$

Thus,

$$\dot{\bar{z}}(t) = \frac{1}{F_n} \int_0^L \frac{\partial z}{\partial t}(\zeta, t) f_n(\zeta) d\zeta \tag{21}$$

After several algebraic manipulations, one obtains the following lumped LuGre tire friction model

$$\dot{\bar{z}}(t) = v_r - \frac{\sigma_0 |v_r|}{g(v_r)} \bar{z}(t) - \kappa(t) |\omega r| \bar{z}(t) \tag{22}$$

$$F(t) = \left(\sigma_0 \bar{z}(t) + \sigma_1 \dot{\bar{z}}(t) + \sigma_2 v_r\right) F_n \tag{23}$$

where $\kappa(t)$ is defined as:

$$\kappa(t) = \frac{1}{F_n \bar{z}} \left\{ \left[z(\zeta, t) f_n(\zeta) \right]_0^L - \int_0^L z(\zeta, t) \frac{\partial f_n(\zeta)}{\partial \zeta} d\zeta \right\} \tag{24}$$

Although κ depends on the normal force distribution, it turns out that in practice the following constant expression

$$\kappa(t) = \frac{\kappa_0(t)}{L}, \quad \kappa_0 \in [1, 2] \tag{25}$$

provides sufficiently accurate results.

We validated the previous theoretical developments via a series of experimental results. Specifically, measurements were collected during three brakings of a specially equipped test vehicle (Fig. 8). The measurements for the three brakings were taken under the same vehicle operational and road conditions. We have used this data to identify the parameters of the average/lumped LuGre tire friction model. We then used these parameters to validate the dynamic friction model by comparing the time histories of the friction force predicted by our model with the friction force measured during the experiments.

The friction data were collected using the "BASIL" car which is a laboratory vehicle based on a Renault Mègane 110 Kw. The car is equipped with several sensors to study the behaviour of the vehicle during braking and traction phases. A schematic of the completely equipped "BASIL" vehicle, along with the corresponding measurement parameters is given in Fig. 8.

The comparison between the experimental results and the simulation results using the LuGre dynamic friction model for the three braking cases are shown in Figs. 10-11.

These figures indicate that our proposed model captures very well both steady-state and transient friction force characteristics.

The results of this work are documented in [30, 31, 3].

2.3 Development of Dynamic Friction Models for Longitudinal/Lateral Motion

In this work we developed an extension to the LuGre dynamic friction model from longitudinal to longitudinal/lateral motion. Application of this model to a tire yields a pair of partial differential

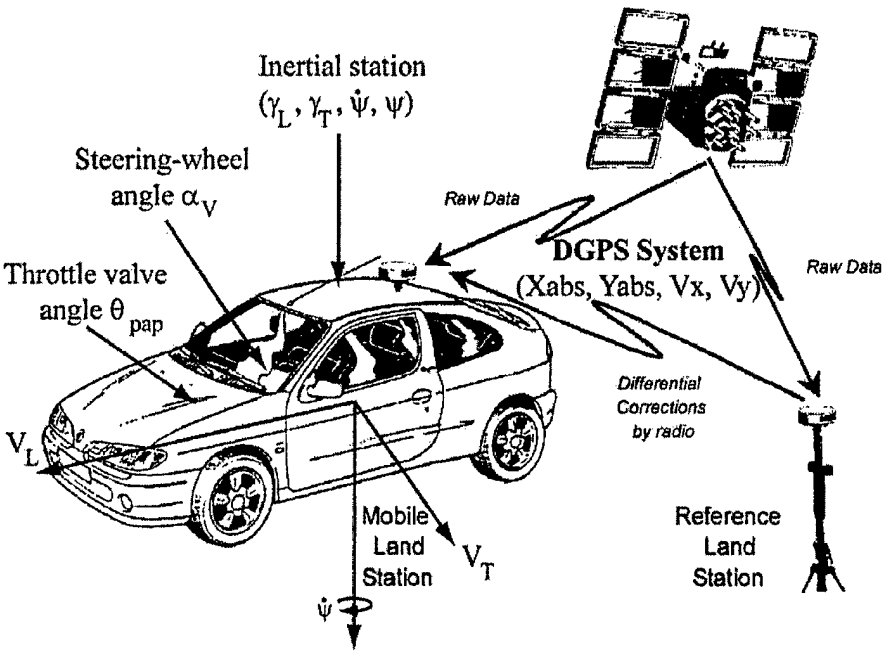

Figure 8: Sensors and measurement parameters; from [3].

equations that model the tire-road contact forces and aligning moment. By the introduction of a set of mean states we reduce the partial differential equation to a lumped model governed by a set of three ordinary differential equations. Such a lumped form describes the aggregate effect of the friction forces and moments and it can be useful for control design and on-line estimation. A method to incorporate wheel rim rotation is also discussed.

We start by introducing a point LuGre 2D model. The proposed friction model is written as follows

$$\dot{z}_i = v_{ri} - C_{0i}(v_r) z_i \tag{26a}$$

$$\mu_i = -\sigma_{0i} z_i - \sigma_{1i} \dot{z}_i - \sigma_{2i} v_{ri} \tag{26b}$$

where,

$$C_{0i}(v_r) = \frac{\lambda(v_r)\sigma_{0i}}{\mu_{ki}^2}, \qquad i = x, y \tag{27}$$

The scalar function $\lambda(v_r)$ is given by

$$\lambda(u, \dot{u}, \mu^*) = \lambda(\dot{u}) := \frac{\|M_k^2 \dot{u}\|}{g(\dot{u})} \tag{28}$$

and the function $g(v_r)$ by

$$g(\dot{u}) = \frac{\|M_k^2 \dot{u}\|}{\|M_k \dot{u}\|} + \left(\frac{\|M_s^2 \dot{u}\|}{\|M_s \dot{u}\|} - \frac{\|M_k^2 \dot{u}\|}{\|M_k \dot{u}\|} \right) e^{-\left(\frac{\|\dot{u}\|}{v_s}\right)^\gamma} \tag{29}$$

where M_s is the matrix of static friction coefficients as in

$$M_s = \begin{bmatrix} \mu_{sx} & 0 \\ 0 & \mu_{sy} \end{bmatrix} > 0 \,, \tag{30}$$

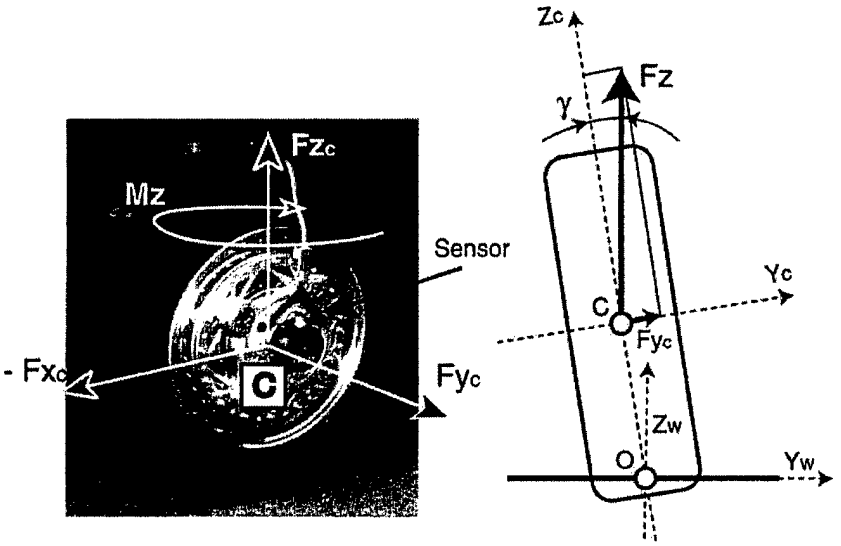

Figure 9: View of the equipped wheel with the Wheel Force Transducer (WFT); variables measured and axis systems used are according to ISO 8855 specifications. Rim and wheel dynamics are neglected so that the FWT forces are related to the actual forces at the contact patch via a simple coordinate transformation; from [3].

Observe that the forces in the x and y directions are coupled due to $\lambda(v_r)$.

We next applied the previous LuGre friction model for 2D motion, in order to derive a model for the tire-road contact forces and moments due to friction. We follow an approach similar to that in [32, 33]. To this end, we assume that the contact patch of the tire (the area of contact with the road) is rectangular (Fig. 12). We divide the contact patch into infinitesimal elements. For each element we apply the point LuGre model for 2D motion of equations (26)-(27). In order to find the total forces and moments we then integrate the forces of each element along the patch. It should be mentioned that although we will keep referring to this friction model as 2D model, it will be in fact a 3-dof model since not only the longitudinal and lateral forces but the aligning moment will be captured as well.

The distributed friction model is summarized by the following equations

$$\frac{\mathrm{d}z_i(t,\zeta)}{\mathrm{d}t} = \frac{\partial z_i(t,\zeta)}{\partial t} + \frac{\partial z_i(t,\zeta)}{\partial \zeta}|\omega r| = v_{ri} - C_{0i}(v_r)z_i(t,\zeta) \tag{31a}$$

$$\mu_i(t,\zeta) = -\sigma_{0i}z_i(t,\zeta) - \sigma_{1i}\frac{\partial z_i(t,\zeta)}{\partial t} - \sigma_{2i}v_{ri}, \tag{31b}$$

where $i = x, y$. The total forces along the x and y directions are computed from

$$F_i(t) = \int_0^L \mu_i(t,\zeta) f_n(\zeta)\mathrm{d}\zeta, \quad i = x, y \tag{32}$$

where $f_n(\zeta)$ is the normal load distribution (force per unit length) along the contact patch and L is the length of the patch. The force distribution along the y direction also results into a moment about the center of the patch (aligning torque) given by

$$M_z(t) = -\int_0^L \mu_y(t,\zeta) f_n(\zeta)\left(\frac{L}{2} - \zeta\right)\mathrm{d}\zeta \tag{33}$$

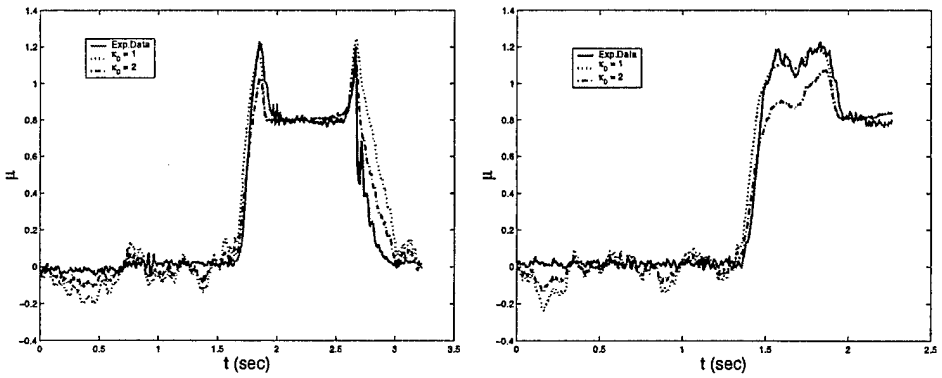

(a) Braking #1 (b) Braking #2

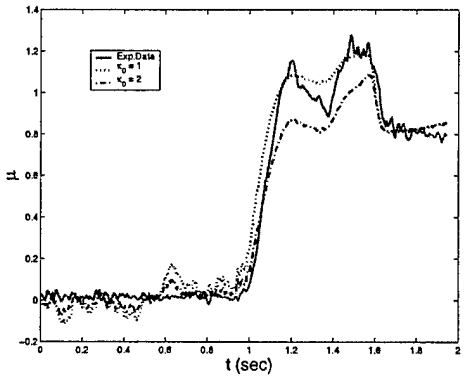

(c) Braking #3

Figure 10: Experimental and simulation results. Case (i): constant $\kappa_0 = 1, 2$; from [3].

Here v_{rx} and v_{ry} are the relative velocity components of the elements in the contact patch with respect to the ground, that is,

$$v_{rx} = \omega r - v\cos(\alpha) \tag{34a}$$

$$v_{ry} = -v\sin(\alpha) \tag{34b}$$

To evaluate this distributed model we compare it against other tire models. In particular, we have made comparison with Pacejka's Magic Formula (MF) model [5] under steady-state conditions. The results are shown in Figs. 13, 14 and 15.

The previous distributed model (31) may not be easy to use for analysis and–most importantly–control design. For this reason, we also developed a lumped model, described by a single ordinary differential equation, which captures the "average" behavior of the internal friction states. It is used to approximate the longitudinal and lateral forces as well as the aligning torque as a function of these "average states," at least at steady-state. The approach used mimics the one used in Refs. [32, 33] for the longitudinal case.

The average lumped model for the friction forces is summarized by the following equations.

$$\dot{\bar{z}}_i(t) = v_{ri} - C_{0i}(v_r)\bar{z}_i(t) - \kappa_i(t)|\omega r|\bar{z}_i(t) \tag{35}$$

$$\bar{F}_i(t) = -F_n(\sigma_{0i}\bar{z}_i(t) + \sigma_{1i}\dot{\bar{z}}_i(t) + \sigma_{2i}v_{ri}), \quad i = x, y. \tag{36}$$

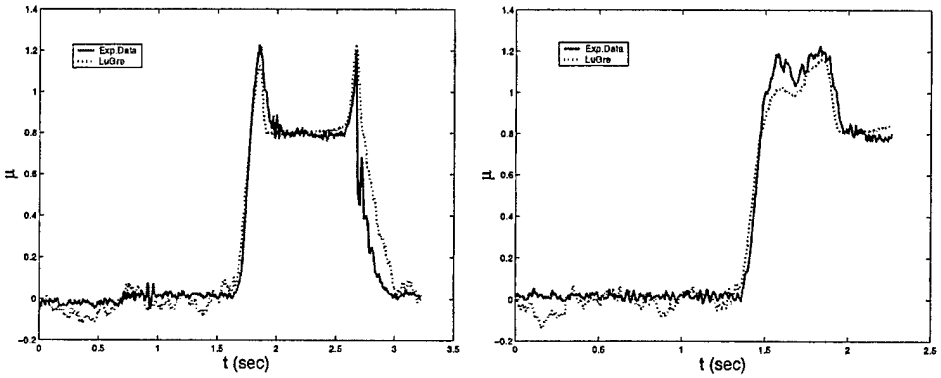

(a) Braking #1 (b) Braking #2

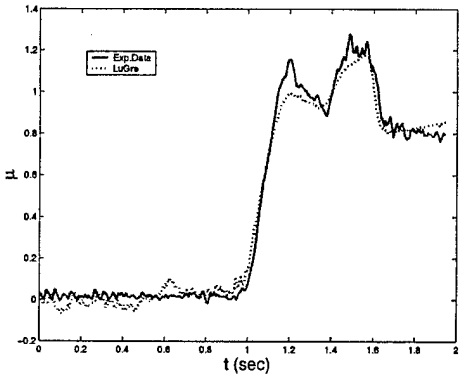

(c) Braking #3

Figure 11: Experimental and simulation results. Case (ii): varying κ_0; from [3].

The average lumped model for the aligning torque is summarized by

$$\dot{\hat{z}}_y(t) = \frac{G}{F_n L} v_{ry} - C_{0y}(v_r)\hat{z}_y(t) - \nu(t)|\omega r|\hat{z}_y(t) + \frac{|\omega r|}{L}\bar{z}_y(t) \tag{37}$$

$$\begin{aligned} \frac{\hat{M}_z(t)}{F_n L} &= \sigma_{0y}\left(\tfrac{1}{2}\bar{z}_y(t) - \hat{z}_y(t)\right) + \sigma_{1y}\left(\tfrac{1}{2}\dot{\bar{z}}_y(t) - \dot{\hat{z}}_y(t)\right) \\ &+ \sigma_{2y}\left(\tfrac{1}{2}v_{ry} - \frac{G}{F_n L}\right). \end{aligned} \tag{38}$$

The results of this work have been documented in [4].

2.4 Exact Transient Tire Friction Dynamics for High-Speed Vehicles

The LuGre dynamic point contact friction model for the two-dimensional translation of a body on a surface has been used to derive a model for the friction forces and moments at the contact patch of a tire. The resulting tire friction model is distributed, i.e., is described by a set of partial differential equations. Several approximations have been developed to approximate this distributed model using a set of ordinary differential equations. Such a lumped form makes the model more suitable for the development and implementation of on-line estimation and control algorithms [34, 35, 36].

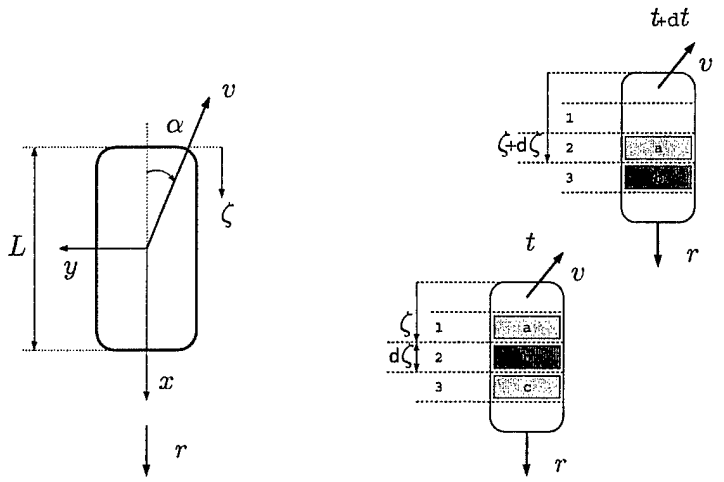

Figure 12: Frames of reference and velocities at the contact patch.

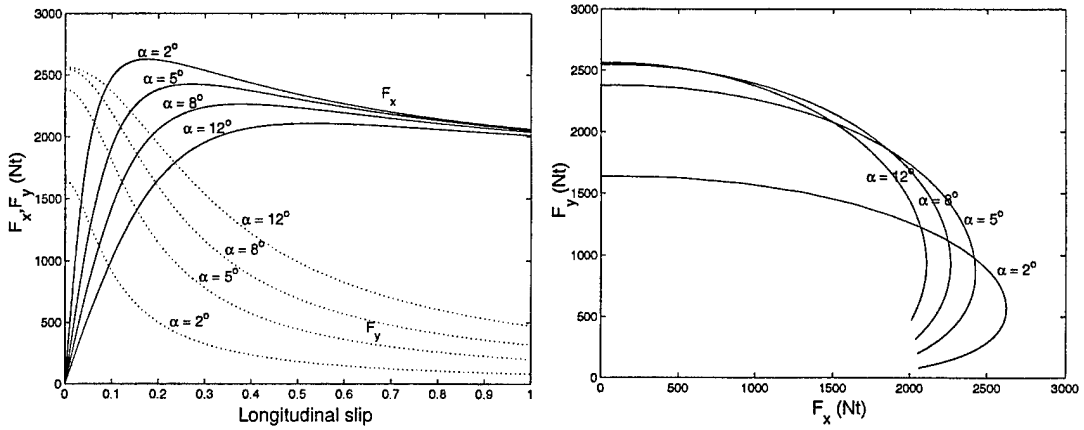

Figure 13: Steady-state forces for several constant values of the slip angle; from [4].

The main objective of the lumped model in [37, 38, 39] was to be able to capture the steady-state behavior of the distributed model exactly. Therefore, this model does not offer any guarantees on the accuracy of the transient dynamics.

In this work the method of moments was used to derive a set of ordinary differential equations to describe the *exact* average dynamics of the distributed model. Three cases of normal load distribution were considered and compared with each other: uniform, trapezoidal and quartic load distribution. Simulations compared with existing approximate lumped models.

The method of moments approach proceeds as follows. First, we define the pth moment of $z_i(t, \zeta)$ for $\zeta \in [a, b]$ as follows

$$M_{p,i}^{ab}(t) := \int_a^b z_i(t, \zeta)\zeta^p \mathrm{d}\zeta, \quad i = x, y \tag{39}$$

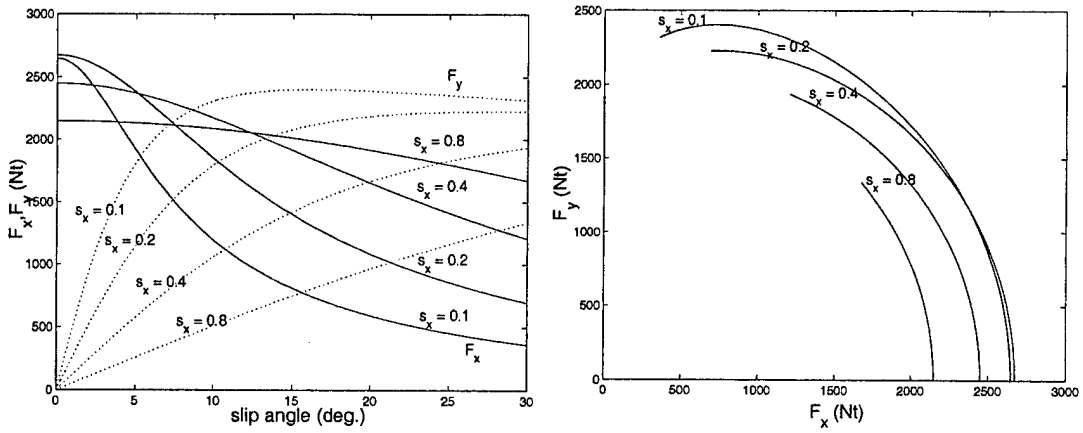

(a) (b)

Figure 14: Steady-State forces for several constant values of the longitudinal slip; from [4].

Taking the time derivative of $M_{p,i}^{ab}$ yields,

$$\begin{aligned}
\dot{M}_{p,i}^{ab}(t) &= \int_a^b \frac{\partial z_i(t,\zeta)}{\partial t}\zeta^p \mathrm{d}\zeta \\
&= \int_a^b \left(v_{ri} - C_{0i}(v_r) z_i(t,\zeta) - |\omega r| \frac{\partial z_i(t,\zeta)}{\partial \zeta} \right) \zeta^p \mathrm{d}\zeta \\
&= \frac{b^{p+1} - a^{p+1}}{p+1} v_{ri} - C_{0i}(v_r) \int_a^b z_i(t,\zeta)\zeta^p \mathrm{d}\zeta \\
&\quad - |\omega r| \int_a^b \frac{\partial z_i(t,\zeta)}{\partial \zeta}\zeta^p \mathrm{d}\zeta. \qquad (40)
\end{aligned}$$

Integrating by parts, (40) gives a recursive formula for the calculation of all moments $M_{p,i}^{ab}$ for $p \geq 1$

$$\begin{aligned}
\dot{M}_{p,i}^{ab} &= \frac{b^{p+1} - a^{p+1}}{p+1} v_{ri} - C_{0i}(v_r) M_{p,i}^{ab} - |\omega r| z_i(t,\zeta)\zeta^p \Big|_a^b \\
&\quad + |\omega r| p M_{p-1,i}^{ab} \qquad (41)
\end{aligned}$$

For $p = 0$ equation (40) yields

$$\dot{M}_{0,i}^{ab} = (b-a) v_{ri} - C_{0i}(v_r) M_{0,i}^{ab} - |\omega r| \Big(z_i(t,b) - z_i(t,a) \Big) \qquad (42)$$

Given any sufficiently smooth normal load distribution $f_n(\zeta)$, we can approximate f_n with its Taylor series expansion as follows

$$f_n(\zeta) \simeq \sum_{k=0}^{m} c_k \zeta^k \qquad (43)$$

for some constants $c_0, c_1, ..., c_m$. Note that the total normal load on the contact patch is given by

$$F_n = \int_0^L f_n(\zeta) \mathrm{d}\zeta. \qquad (44)$$

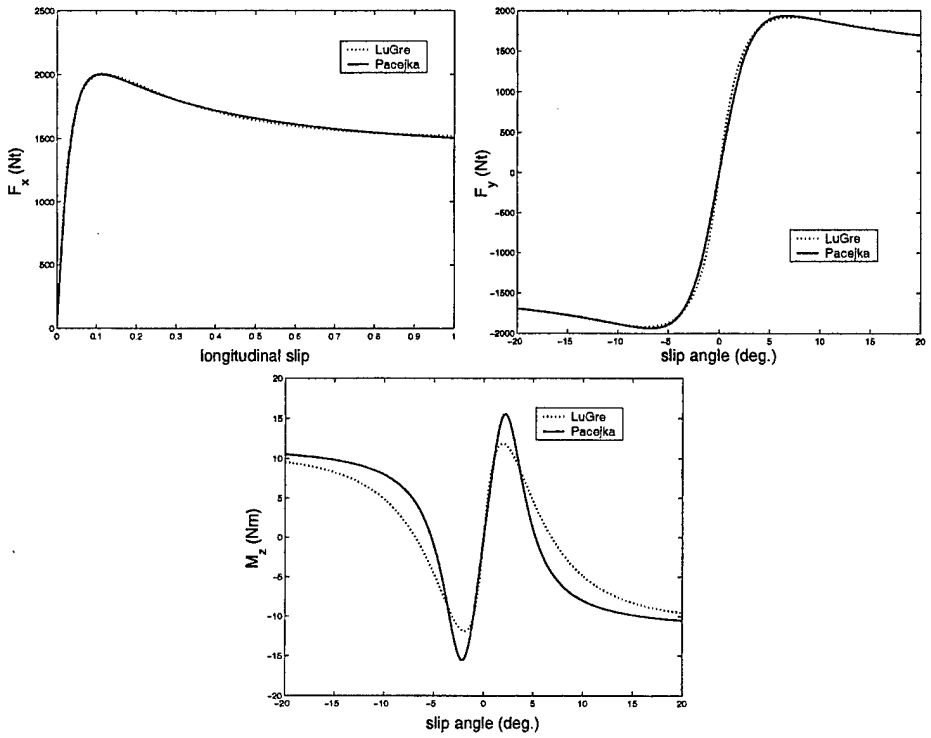

Figure 15: Comparison between LuGre and Pacejka (Magic Formula) models. The values of the parameters for the Magic Formula were taken from [5] and correspond to experimental data; from [4].

Using the definition of the moments $M_{p,i}^{ab}$, and using (43) the friction forces $F_i(t)$ defined by

$$F_i(t) = \int_0^L \mu_i(t,\zeta) f_n(\zeta) \mathrm{d}\zeta, \quad i = x, y \tag{45}$$

can then be written as follows

$$\begin{aligned} F_i(t) &= -\int_0^L \left(\sigma_{0i} z_i + \sigma_{1i} \frac{\partial z_i}{\partial t} + \sigma_{2i} v_{ri} \right) f_n(\zeta) \mathrm{d}\zeta \\ &= -\sigma_{0i} \sum_{k=0}^{m} c_k M_{k,i}^{0L} - \sigma_{1i} \sum_{k=0}^{m} c_k \dot{M}_{k,i}^{0L} - \sigma_{2i} v_{ri} F_n \end{aligned} \tag{46}$$

Finally, the aligning torque $M_z(t)$ defined by

$$M_z(t) = -\int_0^L \mu_y(t,\zeta) f_n(\zeta) \left(\frac{L}{2} - \zeta \right) \mathrm{d}\zeta \tag{47}$$

can be written in terms of the moments $M_{p,i}^{ab}$ as

$$\begin{aligned} M_z(t) &= -\int_0^L \left(\sigma_{0y} z_y + \sigma_{1y} \frac{\partial z_y}{\partial t} + \sigma_{2y} v_{ry} \right) f_n(\zeta) \left(\frac{L}{2} - \zeta \right) \mathrm{d}\zeta \\ &= -\frac{L}{2} F_y(t) + \sigma_{2y} v_{ry} \int_0^L f_n(\zeta) \zeta \mathrm{d}\zeta \\ &\quad + \sigma_{0y} \sum_{k=0}^{m} c_k M_{k+1,y}^{0L} + \sigma_{1y} \sum_{k=0}^{m} c_k \dot{M}_{k+1,y}^{0L} \end{aligned} \tag{48}$$

The normal load along the contact patch has a significant effect on the transient behavior of the friction forces and moments. Several normal load distributions have been used and are shown in Fig. 16, along with a schematic of a realistic load distribution obtained from experiments.

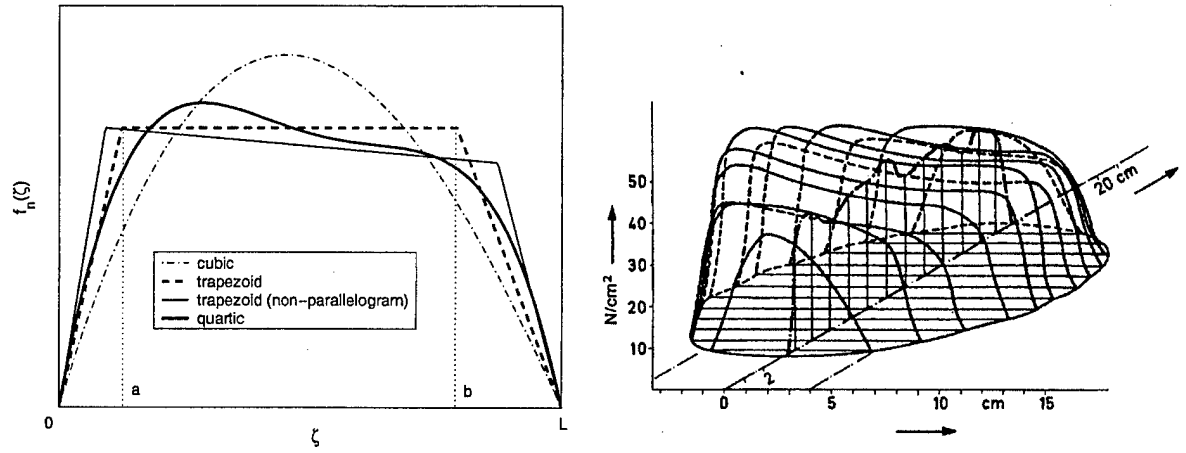

(a) (b)

Figure 16: (a) Possible choices of $f_n(\zeta)$; (b) Empirical plots of normal load distribution taken from [6].

The results of numerical simulations using different load distributions are shown in Fig. 17. We observe that the three normal load models converge to the same steady-state, as expected. However, significant differences in the transient behavior of the three models are also evident. These differences are more apparent in the lateral force F_y and aligning torque M_z. The discrepancy is due to the fact that the normal load distribution $f_n(\zeta)$, along with the distribution of the contact patch deflection $z_i(t, \zeta)$, determine the amount of the total friction generated by each tire element along the contact patch length.

This work has been documented in [40, 7].

2.5 Minimum-Time Vehicle Trajectory Optimization Subject to Friction Constraints

We can distinguish two main approaches followed in the literature to automate vehicle operation. The first approach is to use numerical optimization methods in order to derive the (open-loop) control inputs of the vehicle while driving through a specified path or within some specified state constraints while optimizing the time of travel. The second approach deals with the development of closed-loop control where state-feedback or output-feedback is used to achieve path tracking.

In this work we have performed numerical optimization for a vehicle driving through different types of corners. This allows us to obtain the open-loop control inputs for both longitudinal and lateral control (longitudinal slip and steering angle) for those specific maneuvers. The control inputs obtained can be used directly to control the vehicle if we are confident about the accuracy of the vehicle model and the road description. Such inaccuracies will be dealt with in the future using adaptive control methods. For the time being, we assume that all model parameters are known. The optimal solution obtained can be used as a reference for a path tracking closed-loop controller.

The main differences between our approach to numerical solution of the optimal maneuvering

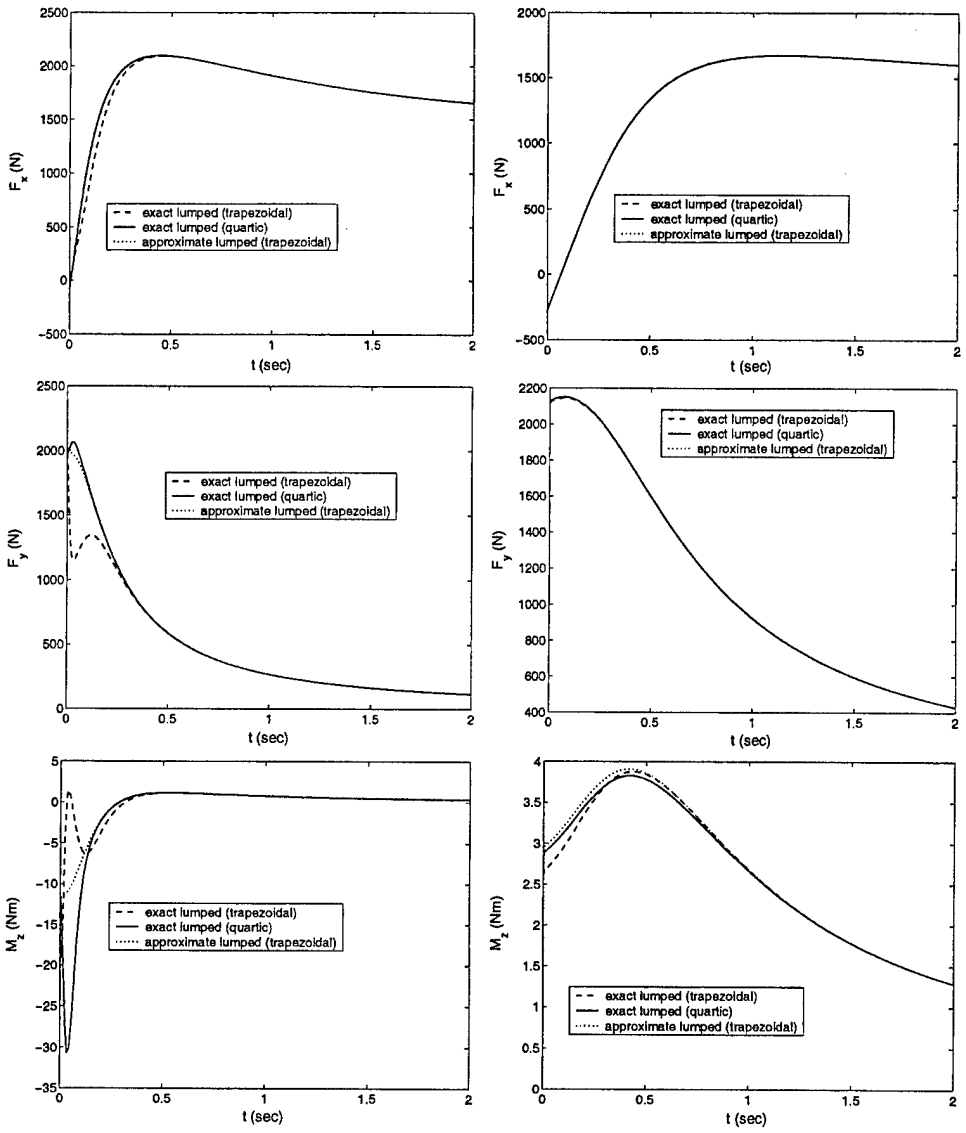

Figure 17: Time histories for longitudinal/lateral forces and aligning torque (trapezoidal and quartic normal load distribution), left column: $\alpha = 4°$, right column: $\alpha = 15°$; from [7].

problem and those in the literature [41], [42] and [43] are as follow. In all the references above, the optimization problem is simplified by a change of the independent variable from time t to traveled distance s. This makes the optimal control problem one of fixed final *time* which is a lot easier to solve numerically. On the other hand this change of variables requires the introduction of a scaling factor including a singularity as mentioned in [42]. The singularity appears when the velocity vector of the car approaches the lateral direction of the vehicle. Such a situation (skidding) is very often intensionally initiated by off-road rally drivers and is expected to appear as part of the optimal solution. In F1 racing skidding is not intended and the optimal solution should be away from the singularity which makes the change of variable in [41], [42] and [43] acceptable. In our case, we want to explore the driving techniques of off-road racing and thus we use time t as the independent variable. Suspension dynamics and longitudinal load transfer are also more dominant in off-road

scenarios where vehicles have "softer" suspensions and higher center of gravity.

To this end we choose a "half-car" description of the vehicle dynamics including suspension dynamics and exact longitudinal load transfer expression, contrary to the description of the vehicle in [42] where a 4-wheel vehicle model is used neglecting suspensions and using an approximation for the load transfer effects. Another difference in our approach is that of the choice of control inputs. In our case we introduce independent longitudinal control in the front and rear axles in order to allow race driving techniques, like "handbrake cornering" and "left foot braking" to appear in the optimal solution. Finally, in our approach we consider different optimization scenarios as far as the cost function is concerned. In particular we investigate optimal time cornering as well as optimal exit velocity cornering.

A typical ground vehicle consists of a main body (frame, passenger area, engine, transmission) linked to four wheels via the suspension system. Except from translation and yawing motion during travel, the suspended body performs pitching, rolling and vertical translation motions. The vehicle interacts with the environment through tire friction forces, which allow the vehicle to accelerate, decelerate and steer as well as aerodynamic drug and lift forces generated due to relative motion of the body and the atmosphere. Steering of the vehicle is generated typically by the front two wheels, although it is not unusual for steering to be generated by the rear or all four wheels. The power is transmitted from the engine to the wheels through the transmission system. Typically, for an off-road vehicle power is transmitted to all four wheels.

A schematic of the half-car model is shown in Fig. 18. The equations of motion are given below.

$$m\ddot{x} = f_{Fx}\cos(\psi+\delta) - f_{Fy}\sin(\psi+\delta) + f_{Rx}\cos\psi - f_{Ry}\sin\psi \quad (49)$$

$$m\ddot{y} = f_{Fx}\sin(\psi+\delta) + f_{Fy}\cos(\psi+\delta) + f_{Rx}\sin\psi + f_{Ry}\cos\psi \quad (50)$$

$$J\ddot{\psi} = (f_{Fy}\cos\delta + f_{Fx}\sin\delta)\,\ell_F - f_{Ry}\ell_R \quad (51)$$

$$I_F\dot{\omega}_F = T_F - f_{Fx}r \quad (52)$$

$$I_R\dot{\omega}_R = T_R - f_{Rx}r \quad (53)$$

In these equations m is the vehicle's mass, J is the polar moment of inertia of the vehicle, I_i, $i = F, R$ are the moments of inertia of the front and rear wheels about the axis of rotation, r is the radius of each wheel, x and y are the cartesian coordinates of the C.G. in the inertial frame of reference, ψ is the yaw angle of the vehicle, ω_i, $i = F, R$ is the angular rate of the front and rear wheel. By f_{ji}, $j = x, y$ and $i = F, R$ we denote the longitudinal and lateral friction of the front and rear wheels, respectively. In this model the inputs are the driving/braking torques T_F and T_R at the front and rear wheels respectively, and δ is the steering angle of the front wheel.

The suspension dynamics are essentially added to the overall vehicle model. They allow one to incorporate the effects of dynamic normal load transfer from one wheel to the others during acceleration/braking and cornering of the vehicle. Normal load transfer appears as a reaction to inertial forces during acceleration when the vertical distance of the center of gravity of the vehicle is taken into consideration. Normal load transfer may be expressed without introducing the additional suspension dynamics, but in this case it is expressed as a function of the derivatives of states of the vehicle model [8]. In some cases, the load transfer is approximated using the vehicle model's inputs and states, as in [44], [42] and [43]. In this work we have proposed to describe the dynamic normal load transfer by introducing the suspension dynamics. No approximation is necessary and the effect is completely described by the states of the system making it possible for the dynamic load transfer effect to be taken into consideration in a simulation scheme. Having already assumed a half-car model, we have investigated the normal load transfer in the longitudinal only direction, that ism load transfer from the front to the rear axle.

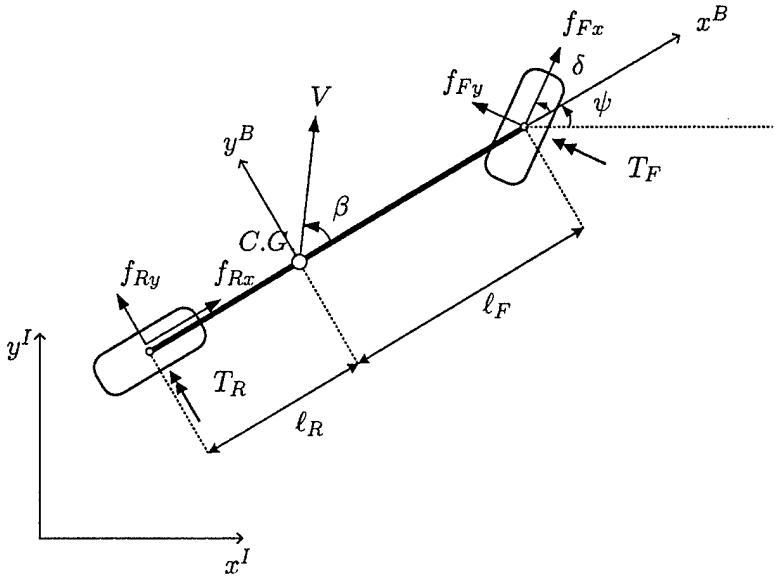

Figure 18: Bicycle Model

In order to incorporate the effect of the transfer load during acceleration and deceleration, let z be the vertical displacement of the center of gravity of the vehicle and θ the pitch angle of the suspended mass as in Figure 19. The dynamics of the vertical and pitching motion of the suspended

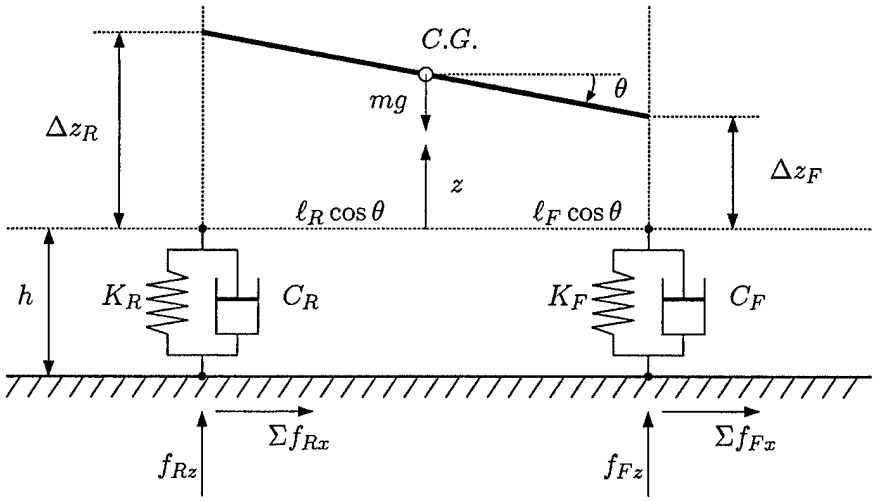

Figure 19: Suspension Dynamics

mass are described by the following equations.

$$m\ddot{z} = f_{Fz} + f_{Rz} - mg \tag{54}$$

$$I_y\ddot{\theta} = f_{Rz}\ell_R\cos\theta - f_{Fz}\ell_F\cos\theta - \Sigma f_{Rx}(h+z) - \Sigma f_{Fx}(h+z) \tag{55}$$

where, m is the vehicle mass (equal to the suspended mass after neglecting the wheel's mass), I_y is the moment of inertial of the vehicle about the center of gravity and the y body axis. By h

we denote the vertical distance of the C.G. from the ground in an equilibrium state where $z = 0$. By $f_{iz}\ \ i = F, R$ we denote the normal load forces at the front and rear axle respectively and by $\Sigma f_{ix}\ \ i = F, R$ we denote the projection of the total friction force of each wheel on the x longitudinal body axis.

$$\Sigma f_{Rx} = f_{Rx} \quad \text{and} \quad \Sigma f_{Fx} = f_{Fx}\cos\delta - f_{Fy}\sin\delta \tag{56}$$

Consider now the equilibrium state ($\dot{z},\ \ddot{z},\ \dot{\theta},\ \ddot{\theta} = 0$) where $z = 0$ and $\theta = 0$. The normal load at each wheel is then the static distribution of the suspended weight to the front and rear axles, which depends on the longitudinal offset of the C.G. In particular we have that

$$f^o_{Fz} = mg\frac{\ell_R}{\ell_F + \ell_R} \tag{57}$$

$$f^o_{Rz} = mg\frac{\ell_F}{\ell_F + \ell_R} \tag{58}$$

Now, given vertical displacement of the C.G. z and pitch angle θ the normal load of each wheel is given by

$$f_{Fz} = f^o_{Fz} - K_F\Delta z_F - C_F\Delta\dot{z}_F \tag{59}$$

$$f_{Rz} = f^o_{Rz} - K_R\Delta z_R - C_R\Delta\dot{z}_R \tag{60}$$

where

$$\Delta z_R = z + \ell_R\sin\theta \quad , \quad \Delta z_F = z - \ell_F\sin\theta$$
$$\Delta\dot{z}_R = \dot{z} + \ell_R\cos\theta\ \dot{\theta} \quad , \quad \Delta\dot{z}_F = \dot{z} - \ell_F\cos\theta\ \dot{\theta}$$

In order to simplify the calculations during the optimization we make some simplifying assumptions which lead to a model of reduced order. The system is presented in equations (49)-(53), (54) and (55) has T_F, T_R and δ as inputs. At this point we make the assumption that we can control the longitudinal slip at each wheel s_{Fx} and s_{Rx} directly. The equations of the system in this case will be

$$m\ddot{x} = f_{Fx}\cos(\psi+\delta) - f_{Fy}\sin(\psi+\delta) + f_{Rx}\cos\psi - f_{Ry}\sin\psi \tag{61}$$

$$m\ddot{y} = f_{Fx}\sin(\psi+\delta) + f_{Fy}\cos(\psi+\delta) + f_{Rx}\sin\psi + f_{Ry}\cos\psi \tag{62}$$

$$J\ddot{\psi} = (f_{Fy}\cos\delta + f_{Fx}\sin\delta)\,\ell_F - f_{Ry}\ell_R \tag{63}$$

The inputs of the system are now the longitudinal slip s_{Fx} and s_{Rx} of the front and rear wheel respectively and the steering angle δ of the front wheel. We may still calculate the "real" inputs T_F and T_R in order to find the angular velocity of each wheel from the known inputs s_{Fx} and s_{Rx}. Differentiating and using equations (52) and (53) we can then calculate the required torques.

Several driving maneuvers have been considered, i.e., 90° corners, U-turns and S-splits both for minimum time and maximum exit velocity. It is noted that minimization of the exposure to danger and reduction of the total mission time requires driving some portions of the trajectory in minimum time while other in maximum velocity. Time minimization and velocity maximization are not necessary the same. Typically, the vehicle would drive faster on a straight path which might not be part of the optimal trajectory for total travel time minimization.

The following boundary conditions have been used, which are summarized in Table 4.

These conditions guarantee that the car is traveling straight before and after the corner. The initial and final position of the car is within the width of the road. Finally, the longitudinal velocities at the initial and final time and the final time t_f are left free. Some representative results from these optimizations are shown in Figs. 20.

Table 4: Boundary Conditions

90° corner	U-turn	S-turn
$x(t=0) = -5$	$-10 \leq x(t=0) \leq -8$	$x(t=0) = -14$
$8 \leq y(t=0) \leq 10$	$y(t=0) = -5$	$-10 \leq y(t=0) \leq -8$
$8 \leq x(t=t_f) \leq 10$	$8 \leq x(t=t_f) \leq 10$	$x(t=t_f) = 14$
$y(t=t_f) = -5$	$y(t=t_f) = -5$	$8 \leq y(t=t_f) \leq 10$
$\psi(t=0) = 0$	$\psi(t=0) = \frac{\pi}{2}$	$\psi(t=0) = 0$
$\dot{\psi}(t=0) = 0$	$\dot{\psi}(t=0) = 0$	$\dot{\psi}(t=0) = 0$
$\psi(t=t_f) = -\frac{\pi}{2}$	$\psi(t=t_f) = -\frac{\pi}{2}$	$\psi(t=t_f) = 0$
$\dot{\psi}(t=t_f) = 0$	$\dot{\psi}(t=t_f) = 0$	$\dot{\psi}(t=t_f) = 0$
$\dot{y}(t=0) = 0$	$\dot{x}(t=0) = 0$	$\dot{y}(t=0) = 0$
$\dot{x}(t=t_f) = 0$	$\dot{x}(t=t_f) = 0$	$\dot{y}(t=t_f) = 0$

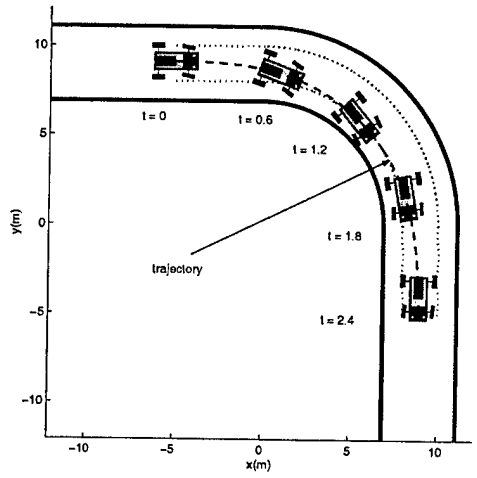

(a) 90° corner, minimum time

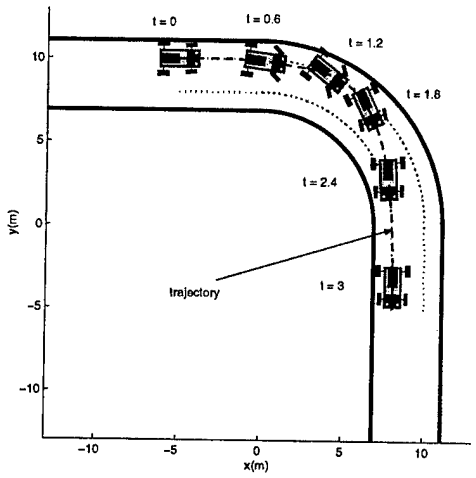

(b) 90° corner, maximum exit velocity

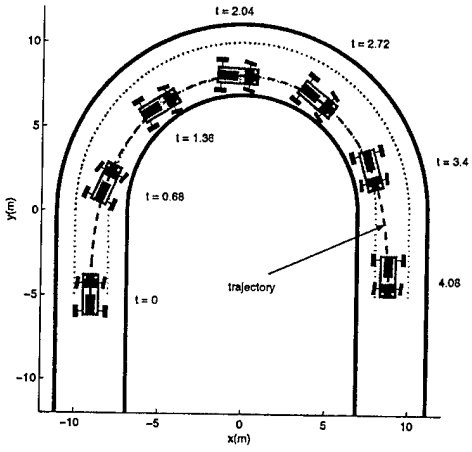

(c) U-turn, minimum time

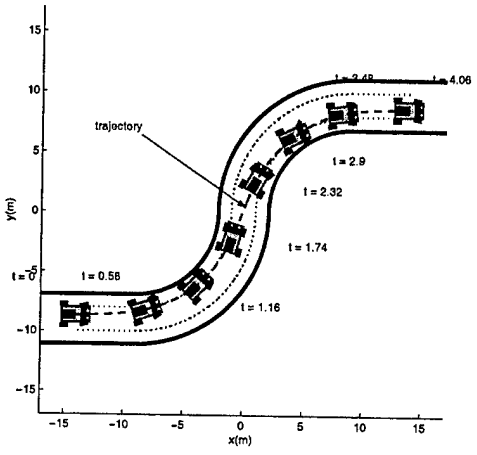

(d) S-turn, minimum time

Figure 20: Optimal vehicle trajectories.

References

[1] B. Kim and P. Tsiotras, "Controllers for unicycle-type wheeled robots: New theoretical results and experimental validation," *IEEE Transactions on Robotics and Automation*, vol. 18, no. 3, pp. 294–307, 2002.

[2] J. Harned, L. Johnston, and G. Scharpf, "Measurement of tire brake force characteristics as related to wheel slip (antilock) control system design," *SAE Transactions*, vol. 78, pp. 909–925, 1969. SAE Paper 6900214.

[3] C. Canudas de Wit, P. Tsiotras, E. Velenis, M. Basset, and G. Gissinger, "Dynamic friction models for road/tire longitudinal interaction," *Vehicle System Dynamics*, vol. 39, no. 3, pp. 189–226, 2003.

[4] E. Velenis, P. Tsiotras, C. Canudas de Wit, and M. Sorine, "Dynamic tire friction models for combined longitudinal and lateral vehicle motion," *Vehicle System Dynamics*, 2004. (to appear).

[5] E. Bakker, L. Nyborg, and H. Pacejka, "Tyre modelling for use in vehicle dynamics studies," *SAE paper # 870421*, 1987.

[6] A. Zomotor, *Fahrwerktechnik: Fahrverhalten.* Vogel Buchverlag Würzburg, 1987.

[7] P. Tsiotras, E. Velenis, and M. Sorine, "A LuGre tire friction model with exact aggregate dynamics," *Vehicle System Dynamics*, 2004. to appear.

[8] W. Milliken and D. Milliken, *Race Car Vehicle Dynamics.* Warrendale PA USA: Society of Automotive Engineers (SAE) International, 1995.

[9] J. B. Pomet, "Explicit design of time-varying stabilizing control laws for a class of controllable systems without drift," *Systems and Control Letters*, vol. 18, pp. 147–158, 1992.

[10] M. R. Murray and S. S. Sastry, "Nonholonomic motion planning: Steering using sinusoids," *IEEE Transactions on Automatic Control*, vol. 38, no. 5, pp. 700–716, 1993.

[11] R. T. M'Closkey and R. M. Murray, "Experiments in exponential stabilization of a mobile robot towing a trailer," in *Proceedings of the American Control Conference*, pp. 988–993, 1994. Baltimore, MD.

[12] A. Teel, R. Murray, and G. Walsh, "Nonholonomic control systems : From steering to stabilization with sinusoids," in *Proceedings of the 31st Conference on Decision and Control*, pp. 1603–1609, 1992. Tuscon, Arizona.

[13] R. T. M'Closkey and R. M. Murray, "Nonholonomic systems and exponential convergence: some analysis tools," in *Proceedings of the 32nd Conference on Decision and Control*, pp. 943–948, 1993. San Antonio, TX.

[14] A. Bloch and S. Drakunov, "Stabilization and tracking in the nonholonomic integrator via sliding modes," *Systems and Control Letters*, vol. 29, pp. 91–99, 1996.

[15] P. Tsiotras and J. Luo, "Reduced-effort control laws for underactuated rigid spacecraft," *Journal of Guidance, Control, and Dynamics*, vol. 20, no. 6, pp. 1089–1095, 1997.

[16] H. Khennouf and C. Canudas de Wit, "On the construction of stabilizing discontinuous controllers for nonholonomic systems," in *IFAC Nonlilear Control Systems Design Symposium*, pp. 747–752, 1995. Tahoe City, CA.

[17] M. Aicardi, G. Casalino, A. Bicchi, and A. Balestrino, "Closed loop steering of unicycle-like vehicles via Lyapunov techniques," *IEEE Robotics and Automation Magazine*, vol. 2, pp. 27–35, 1995.

[18] P. Tsiotras and J. Luo, "Stabilization and tracking of underactuated axi-symmetric spacecraft with bounded inputs," *Automatica*, vol. 36, no. 8, pp. 1153–1169, 2000.

[19] A. Astolfi, "Exponential stabilization of a wheeled mobile robot via discontinuous control," *Journal of Dynamic Systems, Measurements, and Control*, vol. 121, pp. 121–126, 1999.

[20] A. Astolfi, "Discontinuous control of the nonholonomic integrator," in *Modeling and Control of Mechanical Systems* (A. Astolfi, D. Limebeer, and A. Tornambe, eds.), pp. 293–309, June 17-20 1997. Imperial College, London, UK.

[21] R. T. M'Closkey and R. M. Murray, "Exponential stabilization of driftless nonlinear control systems using homogeneous feedback," *IEEE Transactions on Automatic Control*, vol. 42, no. 5, pp. 614–628, 1997.

[22] P. Tsiotras, "Invariant manifold techniques for control of underactuated mechanical systems," in *Modelling and Control of Mechanical Systems* (A. Astolfi, D. Limebeer, and A. Tornambe, eds.), pp. 277–292, June 17-20 1997. Imperial College, London, UK.

[23] B. Kim and P. Tsiotras, "Experimental comparison of control laws for mobile robots," in *8th IEEE Mediterranean Conference on Control and Automation*, July 17–19 2000. Patras, Greece.

[24] B. Kim and P. Tsiotras, "Time-invariant stabilization of a unicycle-type wheeled robot: Theory and experiments," in *IEEE International Conference on Control Applications*, pp. 443–448, Sept. 25–27 2000. Ancorage, AK.

[25] M. Burckhardt, *Fahrwerktechnik: Radschlupfregelsysteme.* Berlin, Germany: Vogel-Verlag, 1993.

[26] E. Bakker, L. Nyborg, and H. Pacejka, "Tyre modelling for use in vehicle dynamic studies." Detroit, MI, 1987. SAE Technical Paper 870421.

[27] A. van Zanten, W. D. Ruf, and A. Lutz, "Measurement abd simulation of transient tire forces," in *International Congress and Exposition*, (Detroit, MI), 1989. SAE Technical Paper 890640.

[28] C. Canudas de Wit, H. Olsson, K. Åström, and P. Lischinsky, "A new model for control of systems with friction," *IEEE Transactions on Automatic Control*, vol. 40, no. 3, pp. 419–425, 1995.

[29] C. Canudas de Wit and P. Tsiotras, "Dynamic tire friction models for vehicle traction control," in *38th IEEE Conference on Decision and Control*, pp. 3746–3751, 1999. Phoenix, AZ.

[30] C. Canudas-de Wit, P. Tsiotras, E. Velenis, M. Basset, and G. Gissinger, "Dynamic friction models for longitudinal road/tire interaction: Experimental results," in *21st IASTED Conference on Modelling, Identification and Control*, Feb. 18–21, 2002. Innsbruck, Austria.

[31] C. Canudas-de Wit, P. Tsiotras, and E. Velenis, "Dynamic friction models for longitudinal road/tire interaction: Theoretical advances," in *21st IASTED Conference on Modelling, Identification and Control*, Feb. 18–21, 2002. Innsbruck, Austria.

[32] C. Canudas de Wit and P. Tsiotras, "Dynamic tire friction models for vehicle traction control," in *Proceedings of 38th IEEE Conference on Decision and Control*, (Phoenix, Arizona, USA), pp. 3746–3751, 1999.

[33] C. Canudas de Wit, P. Tsiotras, E. Velenis, M. Basset, and G. Gissinger, "Dynamic friction models for road/tire longitudinal interaction," *Vehicle System Dynamics*, vol. 39, no. 3, pp. 189–226, 2003.

[34] C. Canudas-de Wit, M. Petersen, and A. Shiriaev, "A new nonlinear observer for tire/road distributed contact friction," in *Proceedings of the* 42^{th} *IEEE Conference on Decision and Control*, December 9-12 2003. Maui, Hawaii, to appear.

[35] C. Canudas de Wit, R. Horowitz, and P. Tsiotras, "Model-based observers for tire/road contact friction prediction," in *New Directions in Nonlinear Observer Design* (H. Nijmeijer and T. Fossen, eds.), vol. 244 of *Lecture Notes in Control and Information Science*, pp. 23–42, London: Springer-Verlag, 1999.

[36] S. Yamazaki, O. Furukawa, and T. Suzuki, "Study on real time estimation of tire to road friction," *Vehicle System Dynamics*, vol. 27, pp. 225–233, 1999.

[37] X. Claeys, C. Canudas de Wit, J. Yi, R. Horowitz, L. Alvarez, and L. Richard, "A new 3d dynamic tire/road friction model for vehicle simulation and control," in *Proceedings of the ASME-IMECE World Conference*, (New York, USA), November 2001.

[38] J. Deur, J. Asgari, and D. Hrovat, "A dynamic tire friction model for combined longitudinal and lateral motion," in *Proceedings of the ASME-IMECE World Conference*, (New York, USA), November 2001.

[39] E. Velenis, P. Tsiotras, and C. Canudas-de Wit, "Extension of the lugre dynamic tire friction model to 2d motion," in *Proceedings of the 10th IEEE Mediterranean Conference on Control and Automation - MED2002*, July 9-12 2002. Lisbon, Portugal.

[40] P. Tsiotras, E. Velenis, and M. Sorine, "A LuGre tire friction model with exact aggregate dynamics," in *American Control Conference*, (Boston, MA), 2004.

[41] J. Hendrikx, T. Meijlink, and R. Kriens, "Application of optimal control theory to inverse simulation of car handling," *Vehicle System Dynamics*, vol. 26, pp. 449–461, 1996.

[42] D. Casanova, R. S. Sharp, and P. Symonds, "Minimum time manoeuvring: The significance of yaw inertia," *Vehicle System Dynamics*, vol. 34, pp. 77–115, 2000.

[43] D. Casanova, R. S. Sharp, and P. Symonds, "On minimum time optimisation of formula one cars: The influence of vehicle mass," in *Proceedings of AVEC 2000*, August 22-24 2000. Ann-Arbor, MI.

[44] R. S. Sharp, D. Casanova, and P. Symonds, "A mathematical model for driver steering control, with design, tuning and performance results," *Vehicle System Dynamics*, vol. 33, pp. 289–326, 2000.

[45] C. Canudas de Wit, P. Tsiotras, X. Claeys, and R. Horowitz, "Friction road/tire modeling, estimation and optimal braking control," in *Proceedings of the Workshop on Automotive Control (NACO2)*, 18-19 May, 2001. Lund, Sweden.

[46] P. Tsiotras and C. Canudas de Wit, "On the optimal braking of wheeled vehicles," in *American Control Conference*, pp. 569–573, June 28–30 2000. Chicago, IL.

[47] E. Velenis, P. Tsiotras, and C. Canudas de Wit, "Extension of the LuGre dynamic tire friction model to 2D motion," in *Proceedings, 10th Mediterranean Conference on Control and Automation (MED2002)*, 2002. Lisbon, Portugal.

3 Research Personnel Supported

Faculty

Prof. Panagiotis Tsiotras, Principal Investigator

Graduate Students

Efstathios Velenis, Ph.D.
Efstathios Velenis, M.S.
Dongwon Jung, M.S.
Kim ByungMoon, M.S.

4 Interactions and Transitions

4.1 Participation and Presentations

The following conferences and workshops were attended:

- *American Control Conference*, Chicago, Illinois, June 28-30, 2000.
- *IEEE International Conference on Control Applications*, Ancorage, Alaska, September 25-27, 2000.
- *Proceedings, 8th IEEE Mediterranean Conference on Control and Automation*, Patras, Greece, July 17-19, 2000.
- *Workshop on Automotive Control*, "Nonlinear and Adaptive Control Network (NACO2)", Lund, Sweden, May 18–19, 2001.
- *21st IASTED Conference on Modelling, Identification and Control*, Innsbruck, Austria, February 18–21, 2002.
- *10th IEEE Mediterranean Conference on Control and Automation (MED2002)*, Lisbon, Portugal, July 9-12, 2002.
- *American Control Conference*, Boston, MA, June 30-July 2, 2004.

Furthermore, conference articles [40, 30, 31, 45, 23, 24, 46, 47] were presented.

4.2 Transitions

The dynamic tire friction models developed under this research award are currently under investigation by the automotive industry (Ford, General Motors) for possible incorporation into the future generation of ABS and TCS for passenger vehicles. It is expected that these models will also be used in high-fidelity simulation environments by the research personnel of TARDEC/TACOM, at Warren, Michigan.

5 Honors and Awards

- Re-Elected to the Editorial Board of *AIAA Journal of Guidance, Control and Dynamics*, 2000–
- Elected to the Editorial Board of *Dynamics and Control: An International Journal*, 2000–2002
- Elected to the Editorial Board of *IEEE Control Systems Magazine*, 2003–
- Elected *Associate Fellow* of the American Instituted of Aeronautics and Astronautics, 2002–
- Elected *Senior Member* of the Institute of Electrical and Electronics Engineers, 2002–

6 Acknowledgment/Disclaimer

This work was sponsored (in part) by the US Army Research Office (ARO), under grant/contract number DAAD19-00-1-0473. The views and conclusions contained herein are those of the author and should not be interpreted as necessarily representing the official policies or endorsements, either expressed or implied, of the US Army Research Office or the U.S. Government.

7 Research Publications and Presentations under this ARO Award

7.1 Doctoral Dissertations and Master's Theses

The following dissertations and theses have directly benefited from the support of this ARO award.

1. "Analysis and Control of High-Speed Autonomous Vehicles," Ph.D. dissertation, (E. Velenis), School of Aerospace Engineering, Georgia Institute of Technology, December 2004 (expected completion date).

7.2 Publications

Book Chapters

1. Canudas de Wit, C., R. Horowitz, and P. Tsiotras, "Model-Based Observer for Tire/Road Contact Friction Prediction," in *New Directions in Nonlinear Observer Design*, Eds: Nijmeijer, H. and T.L. Fossen, *Lecture Notes in Control and Information Science*, Vol. 244, Springer-Verlag, London, May 1999, pp. 23–42.

2. C. Canudas-de-Wit, P. Tsiotras, X. Claeys, J. Yi, and R. Horowitz, "Friction Tire/Road Modeling, Estimation and Optimal Braking Control," in *Nonlinear and Hybrid Systems in Automotive Control*, Eds: Rolf Johansson and Anders Rantzer, *Lecture Notes in Control and Information Science*, Springer-Verlag, London, October 2002, pp. 165–229.

Journal Papers Published in Peer-Reviewed Journals

1. Canudas de Wit, C., Tsiotras, P., Velenis, E., Basset, M. and Gissinger, G., "Dynamic Friction Models for Road/Tire Longitudinal Interaction," *Vehicle System Dynamics*, Vol. 39, No. 3, pp. 189-226, 2003.
2. Kim, B., and Tsiotras, P., "Controllers for Unicycle-Type Wheeled Robots: New Theoretical Results and Experimental Validation" *IEEE Transactions on Robotics and Automation*, Vol. 18, No. 3, pp. 294-307, 2002.
3. Velenis, E., Tsiotras, P., Canudas de Wit, C. and Sorine, M., "Dynamic Tire Friction Models for Combined Longitudinal and Lateral Vehicle Motion," *Vehicle System Dynamics*, (accepted October 2003).
4. Tsiotras, P., Velenis E. and Sorine, M., 'A LuGre Tire Friction Model with Exact Aggregate Dynamics," *Vehicle System Dynamics*, (accepted April 2004).

Conference Proceedings

1. Tsiotras, P. and Canudas de Wit, C., "On the Optimal Braking of Wheeled Vehicles," *Proceedings, American Control Conference*, Chicago, Illinois, June 28-30, 2000, pp. 569–573.
2. Kim, B., and Tsiotras, P., "Time-Invariant Stabilization of a Unicycle-Type Mobile Robot: Theory and Experiments," *IEEE International Conference on Control Applications*, Ancorage, Alaska, September 25-27, 2000, pp. 443–448.
3. Kim, B., and Tsiotras, P., "Experimental Comparison of Control Laws for Mobile Robots," *Proceedings, 8th IEEE Mediterranean Conference on Control and Automation*, Patras, Greece, July 17-19, 2000.
4. Canudas de Wit, C., Tsiotras, P., Claeys, X. and Horowitz, R., "Friction Road/Tire Modeling, Estimation and Optimal Braking Control," *Proceedings of the Workshop on Automotive Control*, "Nonlinear and Adaptive Control Network (NACO2)", Lund, Sweden, May 18–19, 2001.
5. Canudas-de-Wit, C., Tsiotras, P. and Velenis, E., "Dynamic Friction Models for Longitudinal Road/Tire Interaction: Theoretical Advances," *21st IASTED Conference on Modelling, Identification and Control*, Innsbruck, Austria, February 18–21, 2002, pp. 48–53.
6. Canudas-de-Wit, C., Tsiotras, P., Velenis, E., Basset, M. and Gissinger, G. "Dynamic Friction Models for Longitudinal Road/Tire Interaction: Experimental Results," *21st IASTED Conference on Modelling, Identification and Control*, Innsbruck, Austria, February 18–21, 2002.
7. Velenis, E., Tsiotras, P. and C. Canudas de Wit "Extension of the LuGre Dynamic Tire Friction Model to 2D Motion," *Proceedings, 10th Mediterranean Conference on Control and Automation (MED2002)*, Lisbon, Portugal, July 9-12, 2002.
8. Tsiotras, P., Velenis, E. and Sorine, M., "A LuGre Tire Friction Model with Exact Aggregate Dynamics," *American Control Conference*, Boston, MA, June 30-July 2, 2004.